

Bayesian optimisation for Bayesian evidence (BOBE) – a fast and efficient likelihood emulator for model selection

Nathan Cohen^a Jan Hamann^a Ameek Malhotra^b

^aSydney Consortium for Particle Physics and Cosmology, School of Physics, The University of New South Wales, Sydney NSW 2052, Australia

^bPhysics Department, Swansea University, SA28PP, United Kingdom

E-mail: nathan.cohen@unsw.edu.au, jan.hamann@unsw.edu.au,
ameek.malhotra@swansea.ac.uk

Abstract. The formalism of Bayesian model selection provides a very elegant way of ranking different physical models in terms of how compatible they are with a given set of observed data. However, its practical application is often hampered by the challenge of having to compute the Bayesian evidence – a multi-dimensional integral over the product of likelihood and prior probability. This usually necessitates a large number of function calls to the likelihood, which may become prohibitive in case of “slow”, costly to evaluate likelihoods. A possible solution to this problem lies in approximating the slow full likelihood by a fast emulated likelihood. In this paper, we introduce BOBE (Bayesian Optimisation for Bayesian Evidence), a method to construct a Gaussian Process Regression (GPR)-based emulator. BOBE utilises a Bayesian Optimisation algorithm designed specifically to (i) provide a realistic estimate of the emulator’s uncertainty and its impact on the evidence calculation, and (ii) minimise the number of likelihood evaluations required in order to meet a given evidence accuracy goal. We apply it to a number of toy examples as well as actual cosmological likelihoods, and demonstrate that training the emulator to a sufficient accuracy takes a factor of $\mathcal{O}(10^3)$ fewer direct likelihood evaluations than would be needed if one were to directly compute the evidence integral via nested sampling. BOBE’s overhead is independent of the likelihood computation time $t_{\mathcal{L}}$, making it particularly useful for “expensive” likelihoods with $t_{\mathcal{L}} \gtrsim 1$ s. BOBE is written in Python, supports MPI parallelisation, takes advantage of automatic differentiation and just-in-time-compilation provided by JAX, can straightforwardly be implemented with cosmological data analysis frameworks such as Cobaya, and is available for download from <https://github.com/Ameek94/BOBE>.

1 Introduction

At the heart of the empirical sciences lies mankind's desire to understand Nature by describing reality in terms of quantitative theories, i.e., mathematical models. Knowledge can be advanced via the conception of new models on the theory side, or by comparing, ranking or possibly rejecting models in light of new observations. In either case, it is imperative to have rigorous, quantifiable criteria for model selection such that competing theories can be judged fairly.

The framework of Bayesian statistics provides such a criterion, with the fundamental ingredient for Bayesian model comparison being the Bayesian evidence \mathcal{Z} [1–3]. For any given physical model \mathcal{M} with free parameters θ and data \mathcal{D} , it is defined as the integral over the product of the likelihood $\mathcal{L}(\mathcal{D}|\theta, \mathcal{M})$ of the data and the prior probability $\pi(\theta|\mathcal{M})$ of the parameters:

$$\begin{aligned}\mathcal{Z} &\equiv P(\mathcal{D}|\mathcal{M}) = \int d\theta \mathcal{L}(\mathcal{D}|\theta, \mathcal{M}) \pi(\theta|\mathcal{M}) \\ &\equiv \int d\theta \hat{\mathcal{P}}(\theta|\mathcal{M}).\end{aligned}\tag{1.1}$$

Note that the evidence \mathcal{Z} is also the normalisation factor of the posterior probability of the parameters, $\mathcal{P}(\theta|\mathcal{M}) \equiv \frac{1}{\mathcal{Z}} \mathcal{L}(\mathcal{D}|\theta, \mathcal{M}) \pi(\theta|\mathcal{M})$, so one can interpret the integrand of Eq. (1.1) as an unnormalised posterior $\hat{\mathcal{P}}(\theta|\mathcal{M})$. If we assume two models \mathcal{M}_1 and \mathcal{M}_2 with equal model prior probabilities $P(\mathcal{M}_1) = P(\mathcal{M}_2)$, the ratio of two different models' evidences, also known as the Bayes factor,

$$\mathcal{B}_{12} \equiv \frac{\mathcal{Z}_1}{\mathcal{Z}_2} = \frac{P(\mathcal{D}|\mathcal{M}_1)}{P(\mathcal{D}|\mathcal{M}_2)},\tag{1.2}$$

has a natural interpretation in terms of “betting odds” between the models. Unlike frequentist approaches based on maximum likelihood values which only measure the quality of fit at a point, the evidence quantifies how well the model as a whole explains the data. It rewards risky predictions that agree well with the data and punishes generic models which need parameters to be fine-tuned to achieve a good fit, thereby organically implementing the spirit of Occam's razor. Bayes factors are commonly mapped to a strength of the evidence in favour of one model via Jeffreys' scale [2, 4] (see, e.g., Tab. 1).

$\ln \mathcal{B}_{12}$	\mathcal{B}_{12}	Evidence in favour of \mathcal{M}_1
$\ln \mathcal{B}_{12} < 0$	$\mathcal{B}_{12} < 1$	none (\mathcal{M}_2 preferred)
$0 \leq \ln \mathcal{B}_{12} < 1$	$1 \leq \mathcal{B}_{12} \lesssim 3$	inconclusive
$1 \leq \ln \mathcal{B}_{12} < 2.5$	$3 \lesssim \mathcal{B}_{12} \lesssim 20$	weak
$2.5 \leq \ln \mathcal{B}_{12} < 5$	$12 \lesssim \mathcal{B}_{12} \lesssim 150$	moderate
$\ln \mathcal{B}_{12} \geq 5$	$\mathcal{B}_{12} \gtrsim 150$	strong

Table 1. Jeffreys' scale, adapted from Ref. [2].

If one aims to reliably differentiate between different categories on the Jeffreys scale, it follows that the computation of the logarithm of the Bayes factors has an explicit precision requirement of $\mathcal{O}(0.1)$ (which similarly applies to the precision of the log-evidences, $\sigma_{\ln \mathcal{Z}}$).

Generally, the bottleneck of Bayesian model selection lies in the computation of the evidence integral (Eq. (1.1)).¹ Even for basic typical model selection problems encountered in cosmology, efficient state-of-the-art integration methods based on nested sampling [5] (as implemented in packages such as `MultiNest` [6], `Polychord` [7, 8], `Dynesty` [9] or `nautilus` [10]), or using Markov-chain Monte Carlo (MCMC)-generated posterior samples [11–16], reaching an evidence precision of $\sigma_{\ln z} \sim 0.1$ necessitates upwards of 10^5 – 10^6 evaluations of the integrand [17] – a substantially larger number than would be required for parameter inference [18–20].

The number of evidence integral evaluations required by nested sampling and MCMC typically exhibits only mild scaling with the dimensionality of parameter space, as long as the integrand is well-behaved (i.e. unimodal, approximately Gaussian, with linear degeneracies between parameters) [5, 21]. However, likelihoods or priors of higher complexity with features such as multimodality, non-Gaussianity or non-linear degeneracies may lead to a significant increase in the number of function calls needed.

This is not problematic *per se*, but may become an issue when coupled with evidence integrands that are expensive to calculate. Here, the cost of a single evaluation depends both on the model and the observable under consideration. To give an example from a cosmological context, considering *Planck* Cosmic Microwave Background (CMB) anisotropy data [22], computation times for theory plus likelihood on a modern CPU may range from a fraction of a second for base Λ CDM cosmology to $\mathcal{O}(1\text{ s})$ in extended models (e.g., Λ CDM with non-zero spatial curvature [23], or inflationary features [24])). However, for other models or observables where costly non-perturbative simulations must be performed (e.g., N-body [25], hydrodynamics [26], lattice [27] or numerical relativity [28]), it might take hours or even days. In the future, as the precision of observations improves, there will be a trend for the corresponding likelihoods to become more elaborate, necessitating at the same time more accurate (and therefore more expensive) theory calculations, thereby exacerbating the issue.²

A possible solution to this problem lies in replacing the expensive evidence integrand with a fast approximation (a.k.a. emulator or surrogate) that is trained on the real integrand – and then performing the integration as usual, e.g. with nested sampling, on the emulated integrand.

There are many examples of cosmological theory emulators for CMB or matter power spectra, see for instance Refs. [29–39]. Pure theory emulators have the advantage of being applicable to different (combinations of) data sets without having to retrain, though their construction is of course specific to a particular kind of observable, and they may only be of limited use in cases where the computation of the likelihood function itself is expensive. In this work, we opt to emulate the full likelihood³ instead. While such an approach does require separate emulators to be trained for each combination of model and data set under consideration, it also makes the method of emulator construction agnostic to whatever observable the likelihood implicitly depends on. The applicability of our methodology is therefore not limited to problems involving, say, CMB or matter power spectrum data, or cosmology for that matter, but it can be used on any function that is positive definite and integrable over

¹Evaluating the integrand of Eq. (1.1) involves three separate computations: (i) priors $\pi(\theta|\mathcal{M})$ (this is typically trivial), (ii) theory (i.e., the theoretical prediction of observables given parameters θ and model \mathcal{M}) and (iii) likelihood function (which takes as input the observables computed in step (ii)).

²In addition, new data may require the introduction of additional nuisance parameters, causing the dimensionality of the problem to increase as well.

³more precisely, the logarithm of the unnormalised posterior

the support of the prior.

Starting from the assumption of the evidence integrand being expensive to compute, our task is therefore to build an emulator that satisfies the following criteria:

- 1) It is sufficiently precise, i.e. the total evidence uncertainty $\sigma_{\ln \mathcal{Z}}$ should be dominated by the integration uncertainty, not the emulator uncertainty,
- 2) Its construction should endeavour to minimise the number of likelihood computations required to achieve criterion 1), and
- 3) It does not make any prior assumptions about the shape of the likelihood function and is thus applicable to arbitrary likelihoods.

The second criterion disfavours static pre-determined training strategies such as grid scans, Latin hypercube [40–42] or hypersphere [43] sampling or on-the-fly emulation methods with underlying random walk/sampling [38, 39, 44] in favour of training via an active sampling strategy. In other words, we want to employ an algorithm to dynamically choose where to evaluate the next sample, and iteratively “learn” the target function as more samples are collected.

Our guiding principle in designing such an algorithm will be the question: *Given what we know about $\hat{\mathcal{P}}$ from the samples already taken, where should it be evaluated next such that we maximise the expected reduction in the uncertainty of $\ln \mathcal{Z}$?* As we shall discuss in more detail below, an emulator based on Gaussian Process Regression (GPR) [45] combined with a Bayesian Optimisation (BO)-inspired [46–48] active acquisition strategy ideally suits our requirements⁴, as it can be used not only to address this question, but in addition provide us with a reliable convergence diagnostic, i.e., the ability to detect when the emulator meets criterion 1).

GPR with BO has been applied to cosmology for finding likelihood extrema [50] or speeding up parameter inference [51–56]. The framework presented in our work can perform these tasks as well, but its focus lies on facilitating evidence calculations – we thus name it BOBE (Bayesian Optimisation for Bayesian Evidence). A basic flowchart of the BOBE algorithm is shown in Fig. 1.

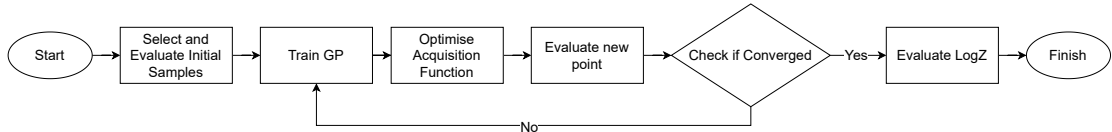


Figure 1. Flowchart of the general BOBE framework for constructing a likelihood emulator and computing the log-evidence.

This paper is structured as follows: in Sec. 2, we provide a brief review of Gaussian Process Regression, followed by a derivation of our acquisition function in Sec. 3 and a description of the BOBE algorithm in Sec. 4. A validation of BOBE, along with an analysis of its efficiency and results of its application to real cosmological problems is presented in Sec. 5 before we conclude in Sec. 6.

⁴See also Ref. [49] for a recent example of a neural network-based likelihood emulator.

2 Gaussian Process Regression

We briefly recap the central concepts underlying Gaussian Process Regression here – for more details the reader is referred to the textbook by Rasmussen and Williams [45]. GPR is a non-parametric regression method that models a real-valued target function $f(\mathbf{x})$, $\mathbf{x} \in \mathbb{R}^{N^5}$ in terms of a Gaussian Process, i.e., one imposes a prior belief that f is described by a collection of jointly Gaussian random variables with mean function $m(\mathbf{x})$ and whose covariance is determined by a kernel function $k(\mathbf{x}, \mathbf{x}')$:

$$f(\mathbf{x}) \sim \mathcal{GP}(m(\mathbf{x}), k(\mathbf{x}, \mathbf{x}')). \quad (2.1)$$

Given a training set \mathcal{T} consisting of n noisy “measurements” of the target function f with iid noise variance σ_n^2 ,

$$\mathcal{T} = \{\mathbf{X}, \mathbf{y}\} \quad \mathbf{X} = [\mathbf{x}_1, \dots, \mathbf{x}_n]^\top, \quad \mathbf{y} = [f(\mathbf{x}_1), \dots, f(\mathbf{x}_n)]^\top, \quad (2.2)$$

the GP prior implies that the training values \mathbf{y} and the function value at a new test point \mathbf{x}_* follow a joint normal distribution:

$$\begin{bmatrix} \mathbf{y} \\ f(\mathbf{x}_*) \end{bmatrix} \sim \mathcal{N}\left(\begin{bmatrix} \mathbf{m}(\mathbf{X}) \\ m(\mathbf{x}_*) \end{bmatrix}, \begin{bmatrix} K(\mathbf{X}, \mathbf{X}) + \sigma_n^2 \mathbb{1} & \mathbf{k}(\mathbf{X}, \mathbf{x}_*) \\ \mathbf{k}(\mathbf{X}, \mathbf{x}_*)^\top & k(\mathbf{x}_*, \mathbf{x}_*) \end{bmatrix}\right), \quad (2.3)$$

where $\{\mathbf{m}(\mathbf{X})\}_p = m(\mathbf{X}_p)$, $\{K(\mathbf{X}, \mathbf{X})\}_{pq} = k(\mathbf{x}_p, \mathbf{x}_q)$ and $\{\mathbf{k}(\mathbf{X}, \mathbf{x}_*)\}_p = k(\mathbf{X}_p, \mathbf{x}_*)$. This in turn implies that at a test point \mathbf{x}_* the result of the regression is the posterior distribution

$$f(\mathbf{x}_*) | \mathcal{T} \sim \mathcal{N}(\mu(\mathbf{x}_*), \sigma^2(\mathbf{x}_*)), \quad (2.4)$$

with the posterior mean $\mu(\mathbf{x}_*)$ and its variance $\sigma^2(\mathbf{x}_*)$ (which quantifies the uncertainty of the regression) given by

$$\mu(\mathbf{x}_*) = m(\mathbf{x}_*) + \mathbf{k}(\mathbf{X}, \mathbf{x}_*)^\top (K(\mathbf{X}, \mathbf{X}) + \sigma_n^2 \mathbb{1})^{-1} (\mathbf{y} - \mathbf{m}(\mathbf{X})), \quad (2.5)$$

$$\sigma^2(\mathbf{x}_*) = k(\mathbf{x}_*, \mathbf{x}_*) - \mathbf{k}(\mathbf{X}, \mathbf{x}_*)^\top (K(\mathbf{X}, \mathbf{X}) + \sigma_n^2 \mathbb{1})^{-1} \mathbf{k}(\mathbf{X}, \mathbf{x}_*). \quad (2.6)$$

2.1 GP mean, kernel and hyperparameters

Evidently, the above result depends on the choice of GP mean function $m(\mathbf{x})$ and kernel $k(\mathbf{x}, \mathbf{x}')$. By fixing the functional forms of m and k , the problem can be reduced to choosing instead a finite number of hyperparameters ϕ .

If we make the assumption that no part of parameter space is *a priori* preferred over any other, then the natural choice for the GP mean becomes

$$m(\mathbf{x}) = m_0 = \text{const.} \quad (2.7)$$

As for the kernel, many options have been explored in the literature [57]. One can generally expect likelihoods to be continuous, differentiable functions, in which case a Gaussian kernel is a suitable choice:

$$k(\mathbf{x}, \mathbf{x}') = \sigma_f^2 \exp\left[-\frac{1}{2} \sum_{i=1}^N \left(\frac{x_i - x'_i}{\ell_i}\right)^2\right] + \sigma_n^2 \delta(\mathbf{x} - \mathbf{x}'). \quad (2.8)$$

⁵In our case, we identify \mathbf{x} with the model parameters θ and N is the dimensionality of parameter space.

Hyperparameter	Symbol	Value	Bounds
Outputscale	σ_f^2	*	$[10^{-4}, 10^8]$
Correlation scale for θ_i	ℓ_i	*	$[0.01, 10]$
GP mean	m_0	$\frac{1}{n} \sum_{i=1}^n f(\mathbf{x}_i)$	n/a
Noise variance	σ_n^2	10^{-12}	n/a

Table 2. List of GP hyperparameters. An asterisk denotes hyperparameters whose values are determined by maximising their marginalised log posterior Equation (2.10). Though likelihood evaluations are not usually subject to noise, a small non-zero noise variance improves numerical stability. The upper and lower bounds on outputscale and correlation scale are given in terms of standardised input, see Sec. 4.1 for details.

Besides the already mentioned noise variance σ_n^2 , this kernel introduces $N + 1$ additional hyperparameters: the outputscale σ_f^2 which determines the width of the GP prior, and one correlation length parameter ℓ_i for each of the N dimensions of parameter space. Notably, this kernel depends only on distances between points in parameter space, not on location, consistent with our previous assumption that no part of parameter space is *a priori* special.

The quality of a GPR’s fit to the training data can be quantified in terms of the marginal log-likelihood (MLL):

$$\begin{aligned} \ln p(\mathbf{y}|X, \phi) = & -\frac{1}{2} (\mathbf{y} - \mathbf{m}(X))^\top \left(K(X, X) + \sigma_n^2 \mathbf{1} \right)^{-1} (\mathbf{y} - \mathbf{m}(X)) \\ & - \frac{1}{2} \ln \left| K(X, X) + \sigma_n^2 \mathbf{1} \right| - \frac{n}{2} \ln 2\pi. \end{aligned} \quad (2.9)$$

Applying Bayes’ theorem and multiplying the MLL with hyperparameter prior probabilities $p(\phi)$, one obtains a posterior probability density for the hyperparameters given the training data:

$$\ln p(\phi|X, \mathbf{y}) = \ln p(\phi|\mathcal{T}) = \ln p(\mathbf{y}|X, \phi) + \ln p(\phi) + \text{const.} \quad (2.10)$$

By maximising this quantity we can thus let the data decide which values of the hyperparameters are most appropriate.⁶ A summary of our hyperparameters and their treatment can be found in Tab. 2.

2.2 Emulation

Which physical quantity should the target function f be identified with for our purpose? At first glance, one might naïvely pick the integrand of the evidence integral, $\hat{\mathcal{P}}(\theta|\mathcal{M})$. However, there are two major advantages to emulating its logarithm, $\ln \hat{\mathcal{P}}(\theta|\mathcal{M})$, instead [60].

Firstly, this choice ensures that the emulator does not return unphysical negative values for the posterior. Secondly, a given absolute error in $\ln \hat{\mathcal{P}}$ becomes a relative error in $\hat{\mathcal{P}}$ itself, and the corresponding absolute error of $\hat{\mathcal{P}}$ (which is what is relevant for the evidence uncertainty) scales with $\hat{\mathcal{P}}$, i.e., far in the tails of $\hat{\mathcal{P}}$ it will not be necessary for the emulation to be extremely precise.

We do note that $\ln \hat{\mathcal{P}}$ is in principle unbounded from below, and having to cover too large a dynamical range can affect the accuracy of the emulation. However, noting that if $\hat{\mathcal{P}}$ is small enough it becomes essentially indistinguishable from zero, this issue can be addressed by introducing an effective floor by means of a classifier, see Sec. 4.4 for more details.

⁶In a fully Bayesian treatment, one could marginalise $p(\phi|\mathcal{T})$ over ϕ instead [58, 59], but in practice we found that for our problem this yields very little gain at the cost of substantial additional computational overhead.

3 Bayesian Optimisation and the Weighed Integrated log-Posterior Standard Deviation (WIPStd)

As seen above, GPR gives us not only an estimate of the expectation value of the target function, but also an uncertainty, opening up the opportunity to use our knowledge from the GPR to inform an active exploration strategy, in contrast to methods that by construction rely on random sampling or random walks.

Let us designate the GPR output for a training set \mathcal{T}_t of t input data points by $(\mu_t(\mathbf{x}), \sigma_t(\mathbf{x}))$. In Bayesian Optimisation [46–48], the next point at which to evaluate the target function, \mathbf{x}_{t+1} , is determined by extremising an acquisition function $\mathcal{A}(\mathbf{x})$. The choice of acquisition function depends on the problem at hand; common examples include Expected Improvement (EI) [48] for finding the optimum of the target function, or Integrated Posterior Variance (IPV) [61, 62]/Integrated Mean Squared Prediction Error (IMSPE)[63–65] if one aims to maximise reduction in the uncertainty of the target function regression over all of parameter space.

Neither of these are quite ideally suited to our goal of maximising the decrease in the uncertainty of the evidence (i.e., an integral over a nonlinear mapping of the target function). We will therefore proceed to construct our own acquisition function, starting from the estimate of the evidence at iteration t :

$$\mathcal{Z}_t = \int_V d\mathbf{x} e^{\mu_t(\mathbf{x})} \quad (3.1)$$

where V is the domain of prior support. As a rough but conservative estimate, we quantify the effect of $\sigma_t(\mathbf{x})$ on \mathcal{Z}_t by

$$\mathcal{Z}_{t,\pm} = \int_V d\mathbf{x} e^{\mu_t(\mathbf{x}) \pm \sigma_t(\mathbf{x})}. \quad (3.2)$$

Linearising the exponential for $\sigma_t(\mathbf{x}) \ll 1$

$$\mathcal{Z}_{t,\pm} \approx \int_V d\mathbf{x} e^{\mu_t(\mathbf{x})} (1 \pm \sigma_t(\mathbf{x})) \quad (3.3)$$

and introducing the shorthand

$$S_t \equiv \int_V d\mathbf{x} e^{\mu_t(\mathbf{x})} \sigma_t(\mathbf{x}), \quad (3.4)$$

we have at first order in σ

$$\mathcal{Z}_{t,\pm} \approx \mathcal{Z}_t \pm S_t, \quad \ln \mathcal{Z}_{t,\pm} \approx \ln (\mathcal{Z}_t \pm S_t). \quad (3.5)$$

For $S_t \ll \mathcal{Z}_t$ we Taylor-expand the logarithm around $S_t = 0$,

$$\ln (\mathcal{Z}_t \pm S_t) \approx \ln \mathcal{Z}_t \pm \frac{S_t}{\mathcal{Z}_t}. \quad (3.6)$$

The symmetric uncertainty in the log-evidence is then approximately

$$\sigma_{\ln \mathcal{Z}, t} \approx \frac{1}{2} [\ln \mathcal{Z}_{t,+} - \ln \mathcal{Z}_{t,-}] \quad (3.7)$$

$$\approx \frac{1}{2} \left[\ln \mathcal{Z}_t + \frac{S_t}{\mathcal{Z}_t} - \ln \mathcal{Z}_t + \frac{S_t}{\mathcal{Z}_t} \right] = \frac{S_t}{\mathcal{Z}_t} \quad (3.8)$$

$$= \int_V d\mathbf{x} \frac{e^{\mu_t(\mathbf{x})}}{\mathcal{Z}_t} \sigma_t(\mathbf{x}). \quad (3.9)$$

The factor $e^{\mu_t(\mathbf{x})}/\mathcal{Z}_t$ in the integrand is the GP expectation of the (normalised) posterior probability density $\mathcal{P}_t(\mathbf{x})$. So the uncertainty in $\ln \mathcal{Z}_t$ becomes an integral over the GP uncertainty, weighted by the posterior:

$$\sigma_{\ln \mathcal{Z}, t} \approx \int_V d\mathbf{x} \mathcal{P}_t(\mathbf{x}) \sigma_t(\mathbf{x}). \quad (3.10)$$

This explicitly demonstrates the advantage of emulating $\hat{\mathcal{P}}$: we do not require GPR precision to be the same everywhere in parameter space, high precision is only required in regions of high posterior probability.

If we were to augment our training set by adding a new “fantasy” data point $(\mathbf{x}', \mu_t(\mathbf{x}'))$ (i.e., rather than evaluating $f(\mathbf{x}')$, we pretend the function value at \mathbf{x}' is the GPR expectation), and updated the GPR (while keeping the hyperparameters the same), the augmented GP’s standard deviation can be calculated via [45]

$$\sigma_{t+1}^2(\mathbf{x}|\mathbf{x}') = \sigma_t^2(\mathbf{x}) - \frac{\text{cov}(f(\mathbf{x}), f(\mathbf{x}'))^2}{\sigma_t^2(\mathbf{x}')}, \quad (3.11)$$

where

$$\text{cov}_t(f(\mathbf{x}), f(\mathbf{x}')) = \mathbf{k}(\mathbf{x}, \mathbf{x}') - \mathbf{k}(X, \mathbf{x})^\top \left(K(X, X) + \sigma_n^2 \mathbf{1} \right)^{-1} \mathbf{k}(X, \mathbf{x}'). \quad (3.12)$$

The resulting evidence uncertainty upon the addition of the fantasy data point is a function of \mathbf{x}' :

$$\sigma_{\ln \mathcal{Z}, t}(\mathbf{x}') \approx \int_V d\mathbf{x} \mathcal{P}_t(\mathbf{x}) \sigma_{t+1}(\mathbf{x}|\mathbf{x}'). \quad (3.13)$$

We dub the acquisition function defined by Equation (3.13) “Weighted Integrated log-Posterior Standard Deviation” (WIPStd).

In practice, we approximate the WIPStd integral using Monte Carlo (MC) sampling, by drawing M samples $\{\mathbf{x}_j\}_{j=1}^M$ from the posterior \mathcal{P}_t :

$$\sigma_{\ln \mathcal{Z}, t}(\mathbf{x}') \approx \widehat{\mathfrak{W}}(\mathbf{x}') \equiv \frac{1}{M} \sum_{j=1}^M \sigma_{t+1}(\mathbf{x}_j|\mathbf{x}') \quad (3.14)$$

and adopt $\widehat{\mathfrak{W}}(\mathbf{x}')$ as our acquisition function, i.e., the next point to evaluate the target function at is chosen as

$$\mathbf{x}_{t+1} = \arg \min_{\mathbf{x}'} \widehat{\mathfrak{W}}(\mathbf{x}'). \quad (3.15)$$

As only one new observation is being added at a time, we can utilise a rank-one update of the Cholesky factorisation of the kernel matrix, requiring only $\mathcal{O}(N^2)$ operations [48]. Thus, the cost of acquisition function optimisation remains sub-dominant to that of GP training which goes as $\mathcal{O}(N^3)$ [45].

Equation (3.14) highlights another extremely convenient property of this construction, namely that the acquisition function $\widehat{\mathfrak{W}}$ is a direct measure of the log-evidence uncertainty $\sigma_{\ln \mathcal{Z}}$. This means it can also be used to track how well the emulator has converged to the target function and thus help us decide when it is precise enough for our purpose, i.e., when further acquisition of samples becomes unnecessary and the BO loop can be stopped.

4 The BOBE algorithm

In this Section, we provide a more technical discussion of the central ingredients of BOBE and present a pseudocode schematic in Algorithm 1.

4.1 Initialisation

Initial training data: It is not strictly necessary for the algorithm to begin with initial samples of the target function; a GPR without data simply returns the GPR prior. But it is of course also possible, and sometimes advantageous, to start from a non-empty initial training set, for instance if samples from previous runs for the same prior/model/data combination⁷ are available. Or in case one has prior knowledge about characteristics of the target function that are not already represented in the parameter priors, e.g., the (approximate) location of the global posterior maximum, or properties like suspected multimodality. If the GP already knows where the interesting regions of the target function are rather than having to discover them first, the algorithm will tend to converge more quickly and be less likely to suffer from premature convergence.

In addition to permitting starts from a user-supplied training set, BOBE includes options to build an initial training set by generating

- random samples from the prior or an arbitrary user-defined reference distribution, or
- quasi random, low discrepancy Sobol sequence [66] samples over the prior support (see Ref. [67]).

Either of these two options essentially enforces an initial wide exploration of parameter space before active sampling commences. Having too many samples initially generated this way may negatively impact overall efficiency though – we recommend that one should aim to keep the number of initial points below 10–20% of the total likelihood evaluation budget.

Input standardisation: In order to improve numerical stability, we initially map the prior volume of parameter space to the unit hypercube. In addition, we standardise the target function values such that the training points have zero mean and unit variance – this is repeated every time the training set is updated. Internally, the code therefore only deals with standardised input. All quantities are mapped back to their physical values in the final output.

4.2 GP Training

Starting with the initial training set, and every time the training set is expanded, we perform a GPR as outlined in Section 2. The output and correlation scale hyperparameters are determined by applying a gradient-based optimiser (we use the one included in `scipy` [68] by default) to find the values that maximise the MLL. The optimiser is restarted multiple times from random initial points in hyperparameter space, plus one restart from the previous iteration’s optimal values. Hyperparameters typically tend to stabilise once the training set becomes large enough, so it may not be necessary to optimise them (a task that scales like N^3 for a GP with N training points) every single time a sample is added, and BOBE includes an option to do this only every few iterations.

⁷or postprocessed samples for different priors or data

4.3 Acquisition

Evaluating and optimising WIPStd: To evaluate the acquisition function $\widehat{\mathfrak{W}}$, we first generate a set of samples ⁸ from the posterior, utilising either NumPyro’s [69] No-U-Turn (NUTS) Hamiltonian Monte Carlo sampler [70] or the Dynesty [9] nested sampler. $\widehat{\mathfrak{W}}$ as a function of the location of a fantasy observation can then be computed using Equation (3.14). A gradient-based optimiser is then used to find the point that minimises the acquisition function. The coordinates of the minimum specify the point at which the target function will be evaluated next. We illustrate this process for a simple 1-dimensional example in Fig. 2. As we can see in the lower panels, the structure of the acquisition function can become quite complicated as more samples are taken, and it is not unlikely for the optimiser to only discover a local minimum and miss the global one. However, in the long run imperfect optimisation at this step will not pose a major issue for the performance of the algorithm. Eliminating significant local minima of the acquisition function makes discovery of the global minimum more likely in the following iterations, so in most cases this will only affect the order in which points are sampled.

Batch acquisition: Rather than immediately computing the target function after one round of acquisition minimisation, and adding the new data point to the training set, one can also (temporarily) add a fantasy observation at the minimum to the training set and repeat the whole acquisition process, multiple times if desired. This method is also known as the Kriging believer method [55, 71–76] and allows the selection of a whole batch of candidate points for target function evaluation in one go – which has the big advantage of letting us perform expensive target function computation in parallel.

Once a batch is completed, the minimum value of the acquisition function for the final candidate point is retained to be used in the convergence test step, the temporary fantasy points are removed from the training set, and the true $\ln \hat{\mathcal{P}}$ is computed for all candidate points.

4.4 Classifier filtering

In many realistic applications, especially those with higher-dimensional parameter spaces, it is not atypical for the evidence integral to be dominated by the contribution of a small fraction of the prior volume, and for most of the prior volume to be occupied by the tails of the posterior which contain a negligible part of the total evidence. It is therefore unnecessary to aim for a very precise emulation of $\ln \hat{\mathcal{P}}$ in the tails. In fact, it may even be counterproductive to do so, since increasing the range of $\ln \hat{\mathcal{P}}$ one tries to emulate may negatively affect the ability of the GPR to precisely model the important high-posterior regions.

This issue can be avoided by introducing an effective floor for $\ln \hat{\mathcal{P}}$ by means of a classifier that distinguishes between relevant and irrelevant parts of parameter space – an approach that was also used in Gpry [54]. Data points for which $\ln \hat{\mathcal{P}}_{\max} - \ln \hat{\mathcal{P}}$ exceeds a threshold Δ (selected to be large enough such that $\hat{\mathcal{P}}_{\max} e^{-\Delta}$ is functionally indistinguishable from $\hat{\mathcal{P}} = 0$) will not be passed to the GP, and in regions classified as irrelevant, the emulator will set $\ln \hat{\mathcal{P}}$ to the effective floor value $\ln \hat{\mathcal{P}}_{\max} - \Delta$. Details of our implementation are provided in Section A.

⁸When choosing the number of samples, one should aim to have sufficient samples to properly represent the emulated posterior without introducing unnecessary computational overhead in the calculation of the acquisition function. Generally, higher dimensional and more complex target functions require more samples.

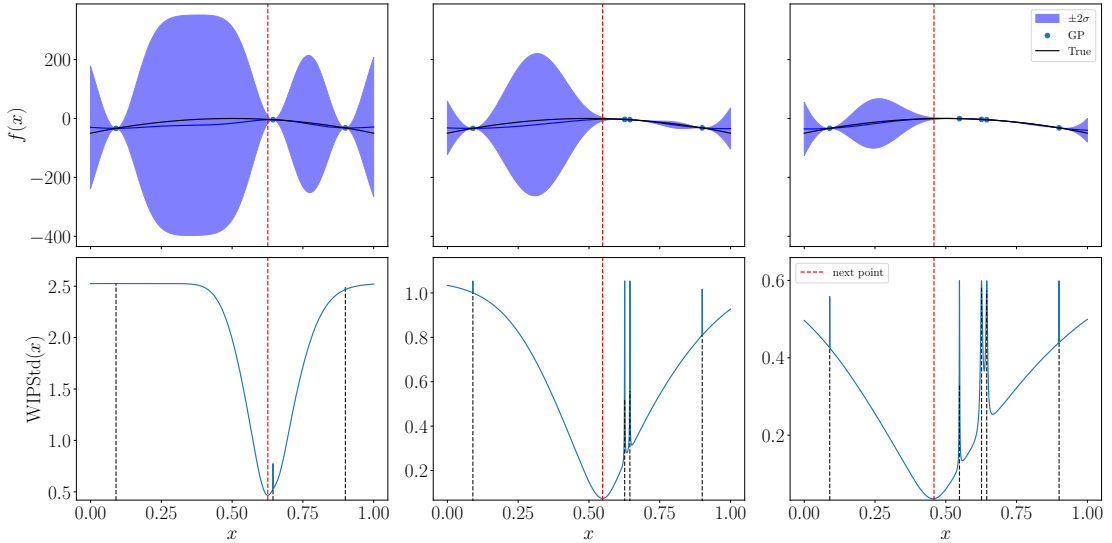


Figure 2. Demonstration of the WIPStd acquisition function in action across three consecutive iterations. **Top row:** objective function (black solid line) and GP mean prediction (blue points) with evaluation locations (blue circles) and $\pm 2\sigma(x)$ GP uncertainty region (blue bands). **Bottom Row:** WIPStd(x), approximated by $\widehat{\mathfrak{W}}(x)$ (light blue solid line) with evaluation locations (grey dashed lines) and location of next evaluation (red dashed line). Note the rapid decrease in WIPStd(x) as additional samples are added

An additional benefit of using a classifier is that it makes the emulator immune to catastrophic failure in cases where the likelihood function should fail and return unphysical values for the log-likelihood (e.g., NaN or $-\infty$) – in this case, the corresponding part of parameter space would be classified as irrelevant, $\ln \hat{P}$ set to the effective floor value and it would not contribute to the evidence.

The classifier is retrained each time the training set is updated. Importantly, no data are discarded in this process; sub-threshold points are simply not given to the GP. However, let us add a cautionary note here: in case of multimodal posteriors, activating the classifier too soon may preclude the discovery of isolated local maxima.

4.5 Convergence

As pointed out in Section 3, WIPStd (and $\widehat{\mathfrak{W}}$) are specifically constructed to approximate the emulator uncertainty $\sigma_{\ln \mathcal{Z}}$, i.e., we can use our acquisition function directly to track the emulator’s convergence. Reliable model comparison demanding an overall log-evidence accuracy of $\mathcal{O}(0.1)$, and the typical integrator accuracy being ~ 0.1 on the log-evidence for numerical integration via nested sampling, suggest that a convergence threshold of $\widehat{\mathfrak{W}} < \mathcal{O}(0.1)$ should be a reasonable convergence criterion for most applications. One can slightly mitigate the risk of possible premature convergence due to a random downward fluctuation in $\widehat{\mathfrak{W}}$ by demanding that $\widehat{\mathfrak{W}}$ be smaller than the convergence threshold for n_{iters} consecutive iterations/batches (in our examples below, the default setting is $n_{\text{iters}} = 2$).

Once the convergence criterion is met, the samples selected in the last iteration are evaluated and added to the training set, the classifier (if used) is retrained and GPR performed one final time. The emulator is now complete and ready to use.

Algorithm 1 Bayesian Optimisation for Bayesian Evidence (BOBE)

Require: Objective function $f(\mathbf{x})$, Precision $\varepsilon > 0$, Batch size B , N_{init} initial samples

- 1: Initialise dataset $\mathcal{T}_{\text{train}} \leftarrow \mathcal{T}_{\text{init}} = \{(\mathbf{x}_i^{(\text{init})}, y_i^{(\text{init})})\}_{i=1}^{N_{\text{init}}}$
- 2: **if** Classifier Enabled **then**
- 3: set classifier threshold γ
- 4: Filter $\mathcal{T}_{\text{train}} : \mathcal{T}_{\text{train}} \leftarrow \{(\mathbf{x}_i, y_i) \in \mathcal{T}_{\text{train}} : y_i > \max_j y_j - \gamma\}$
- 5: **end if**
- 6: Optimise GP hyperparameters $\phi^* \leftarrow \arg \max_{\phi} \ln p(\mathbf{y}_{\text{train}} | X_{\text{train}}, \phi)$ (MLL)
- 7: Update GP model $f_{\text{GP}}(\mathbf{x}) | \mathcal{T}_{\text{train}} \sim \mathcal{GP}(m(\mathbf{x}), k(\mathbf{x}, \mathbf{x}', \theta^*))$
- 8: **while** $\sigma_{\ln \mathcal{Z}} \geq \varepsilon$ **do**
- 9: Draw posterior samples $\{f_{\text{GP}}^{(s)}(\mathbf{x})\}_{s=1}^S$ from $f_{\text{GP}}(\mathbf{x})$
- 10: Initialise batch $\mathcal{B} \leftarrow \emptyset$ and temporary dataset $\mathcal{T}_{\text{train}}^{(1)} \leftarrow \mathcal{T}_{\text{train}}$
- 11: **for** $b = 1$ to B **do**
- 12: Select next batch point: $\mathbf{x}_b = \arg \min_{\mathbf{x}} \widehat{\mathcal{W}}^{(b)}(\mathbf{x})$
- 13: Generate a fantasy observation: $\tilde{y}_b \sim f_{\text{GP}}^{(b)}(\mathbf{x}_b)$
- 14: Temporarily augment: $\mathcal{T}_{\text{train}}^{(b+1)} \leftarrow \mathcal{T}_{\text{train}}^{(b)} \cup \{\mathbf{x}_b, \tilde{y}_b\}$
- 15: Update temporary GP: $f_{\text{GP}}^{(b+1)}(\mathbf{x}) | \mathcal{T}_{\text{train}}^{(b+1)}$, $\mathcal{B} \leftarrow \mathcal{B} \cup \{\mathbf{x}_b\}$
- 16: **end for**
- 17: $\sigma_{\ln \mathcal{Z}} \leftarrow \widehat{\mathcal{W}}^{(B)}(\mathbf{x}_B)$
- 18: Evaluate $y_b = f(\mathbf{x}_b)$ for all $\mathbf{x}_b \in \mathcal{B}$
- 19: Augment the training set: $\mathcal{T}_{\text{train}} \leftarrow \mathcal{T}_{\text{train}} \cup \{(\mathbf{x}_b, y_b)\}_{b=1}^B$
- 20: **if** Classifier Enabled **then**
- 21: Filter $\mathcal{T}_{\text{train}} : \mathcal{T}_{\text{train}} \leftarrow \{(\mathbf{x}_i, y_i) \in \mathcal{T}_{\text{train}} : y_i > \max_j y_j - \gamma\}$
- 22: **end if**
- 23: Optimise GP hyperparameters $\phi^* \leftarrow \arg \max_{\phi} \ln p(\mathbf{y}_{\text{train}} | X_{\text{train}}, \phi)$ (MLL)
- 24: Update GP model $f_{\text{GP}}(\mathbf{x}) | \mathcal{T}_{\text{train}} \sim \mathcal{GP}(m(\mathbf{x}), k(\mathbf{x}, \mathbf{x}', \theta^*))$
- 25: **end while**
- 26: $\ln \mathcal{Z}_{\text{GP}} \leftarrow \text{NestedSample}(f_{\text{GP}}, \pi)$

We then evaluate the Bayesian evidence of the model with a high precision nested sampling run of `Dynesty` [9] on the emulator.⁹ While the BOBE emulator is designed for evidence computations, it can just as well be used for parameter inference, conveniently killing two birds with one stone.

5 Results and Validation

5.1 2-dimensional test functions

To demonstrate the performance of our algorithm, we first consider a set of standard 2-dimensional test functions [77]. While the rather benign 2-dimensional Gaussian serves as a first proof of concept, the Gaussian Ring, Himmelblau's and Eggbox functions introduce various pathologies designed to challenge sampling algorithms. Note that in all the following

⁹If desired for diagnostic reasons, it is of course also possible to compute an evidence estimate with an iteration of the emulator that does not yet meet the convergence criterion.

examples, we take these functions to describe the unnormalised posterior $\hat{\mathcal{P}}$, but GPR is performed on $\ln \hat{\mathcal{P}}$.

Our test functions are defined as follows:

2-dimensional Gaussian:

$$\ln \hat{\mathcal{P}}_{\text{G-2D}}(x_1, x_2) = -\frac{1}{2\sigma^2} \sum_{n=1}^2 (x_n - \mu)^2 \quad (5.1)$$

where $x_1, x_2 \in \{0, 1\}$ and $\mu = 0.5$, $\sigma = 0.1$.

Gaussian Ring:

$$\ln \hat{\mathcal{P}}_{\text{G-R}}(x_1, x_2) = -\frac{1}{2} \left(\frac{\sqrt{(x_1 - 0.5)^2 + (x_2 - 0.5)^2} - 0.2}{0.02} \right)^2, \quad (5.2)$$

where $x_1, x_2 \in \{0, 1\}$.

Himmelblau's Function:

$$\ln \hat{\mathcal{P}}_{\text{H}}(x_1, x_2) = -\frac{1}{2} \left(0.1(x_1 + x_2^2 - 7)^2 + (x_1^2 + x_2 - 11)^2 \right), \quad (5.3)$$

where $x_1, x_2 \in \{-4, 4\}$.

Eggbox:

$$\ln \hat{\mathcal{P}}_{\text{E}}(x_1, x_2) = (2 + \cos(4\pi x_1) \cos(4\pi x_2))^3, \quad (5.4)$$

where $x_1, x_2 \in \{0, 1\}$.

We present our results of applying BOBE on these functions in Figures 3, 4, 5 and 6. There are a few points worth mentioning:

- With the exception of the eggbox, WIPStd tracks quite closely the actual difference between the BOBE evidence estimate and the analytically computed ground truth, showing that it is indeed a well-calibrated measure of error. Note that the difference to the ground truth is affected by both emulator error (which on average decreases as we take more samples) and integrator error (which has a constant expectation value of ~ 0.1 .) The total error therefore saturates around 0.1, as clearly visible in Figure 6.
- In all four examples, the final BOBE estimate of the evidence agrees with the true evidence within the integration error.
- The eggbox proves to be a particularly challenging problem, as all 13 modes need to be discovered for an accurate result. We therefore started with a particularly large number of Sobol samples (so that some, but not all, of the modes are known initially), and chose much stricter convergence criteria, to force the code to continue running until all modes are detected and explored.
- In all four examples, it is apparent that the “interesting” parts of the functions (that have either high posterior values or a large gradient) are much more densely sampled than the regions of low posterior.

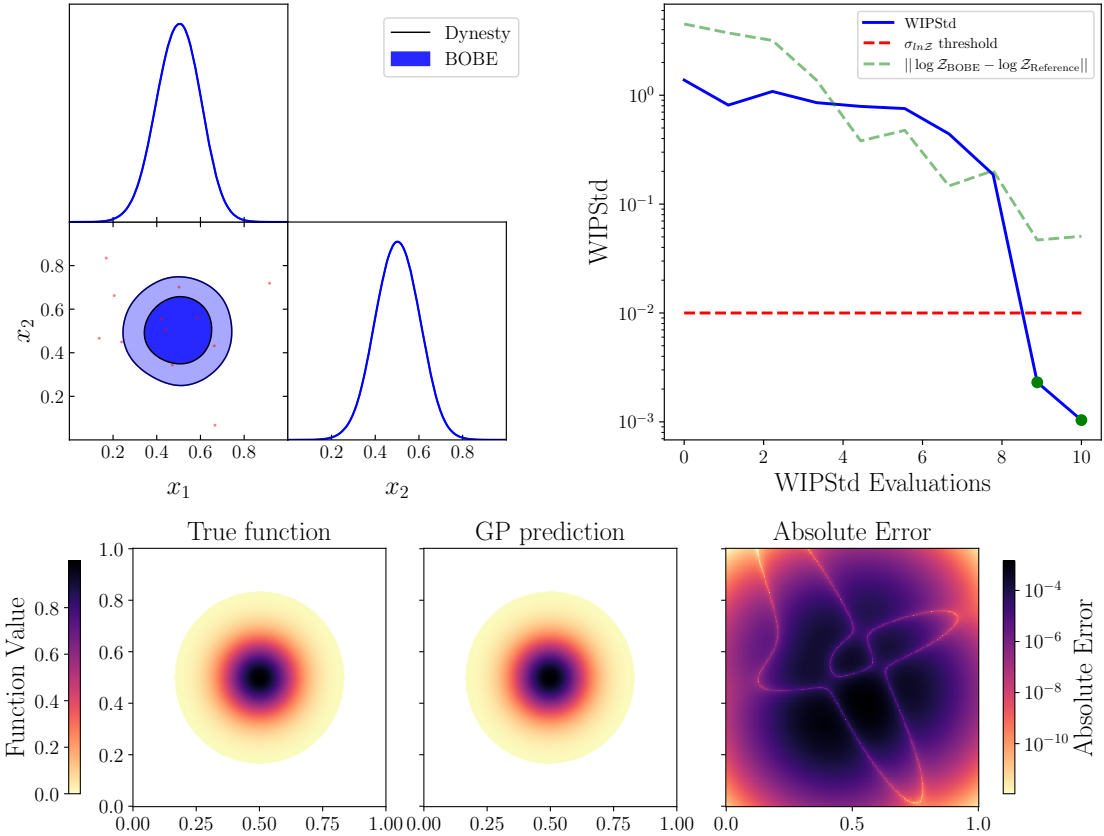


Figure 3. BOBE applied to a 2D Gaussian posterior. **Top Left:** Triangle plot comparing 1D and 2D posteriors contours obtained from the BOBE emulator (blue blobs/lines) and the true posterior (black lines). Locations of the training samples are indicated by red dots. **Top Right:** WIPStd convergence diagnostic (solid blue line) compared with the absolute difference between BOBE evidence estimate and the analytic evidence reference value (green dashed line), plotted as a function of the number of BO iterations. The red dashed line denotes the convergence criterion. **Bottom Row:** Grid evaluations of the true function (left), BOBE GP predictive mean (centre) and their difference (right). The run was initialised with 2 Sobol samples.

- As expected, the absolute accuracy of the emulated posterior is highest in the low-posterior regions.
- There is excellent agreement between the reconstructed 1D and 2D posteriors obtained from sampling the BOBE emulator and the true posterior, demonstrating that BOBE can be used for inference as well.

5.2 N -dimensional Gaussian: scaling with dimensionality

Next we investigate how BOBE’s performance scales with the dimensionality of parameter space. Motivated by the fact that multivariate near-Gaussian posteriors are common in cosmological contexts, we consider for this analysis an N -dimensional Gaussian posterior,

$$\ln \hat{\mathcal{P}}_{G-ND}(\mathbf{x}) = -\frac{1}{2\sigma^2} \sum_{i=1}^N (x_i - \mu)^2 \quad (5.5)$$

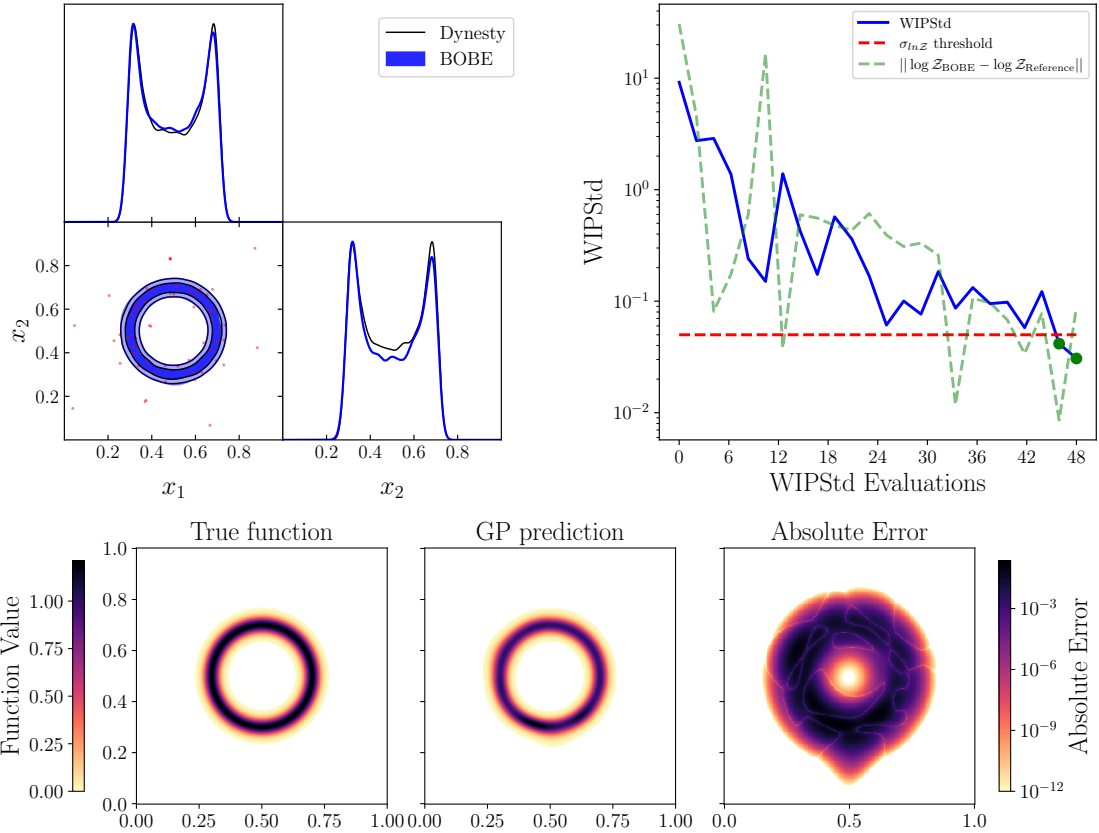


Figure 4. Same as Figure 3 for the Gaussian ring. This run was initialised with 8 Sobol samples.

with $\mu = 0.5$, $\sigma = 0.1$, $x_i \in \{0, 1\}$, and run **BOBE** until a target precision of $\sigma_{\ln Z} \approx \widehat{\mathfrak{W}} = 0.1$ is reached.

The focus here will in particular be on the total number of function calls to the posterior required for **BOBE** to converge (as minimising this quantity was one of our design goals). We compare this with how many function calls would be required if one instead were to follow the standard way of computing evidences, i.e., by using a nested sampler (**Dynesty**, with an integration precision of $\sigma_{\ln Z} = 0.1$) directly calling the likelihood.

Our results for the number of posterior calls up to $N = 35$ dimensions are presented in Figure 7. It is clear that building the **BOBE** emulator is substantially more efficient by this metric than nested sampling with direct calls to the posterior, requiring $\mathcal{O}(10^3)$ fewer evaluations. Since **BOBE** does have a larger computational overhead than nested samplers, this does not directly translate to the same factor in terms of computational time required (though in the limit of sufficiently expensive likelihoods it will¹⁰).

Both **BOBE** and **Dynesty** require more function calls with increasing N . **BOBE**'s scaling is slightly less favourable, but a rough extrapolation of the Figure 7 suggests that it will enjoy a higher efficiency well beyond $N \sim 100$ dimensions.

In the context of the N -dimensional Gaussian case, it may also be enlightening to inspect

¹⁰If one is concerned with overall computation time, the breakeven point in terms of a single likelihood evaluation time $t_{\mathcal{L}}$ depends on the computing hardware and N – in our examples it lies around $t_{\mathcal{L}} \sim 10^{-2}$ to 10^{-1} s, i.e., for likelihoods slower than this, **BOBE** will be faster.

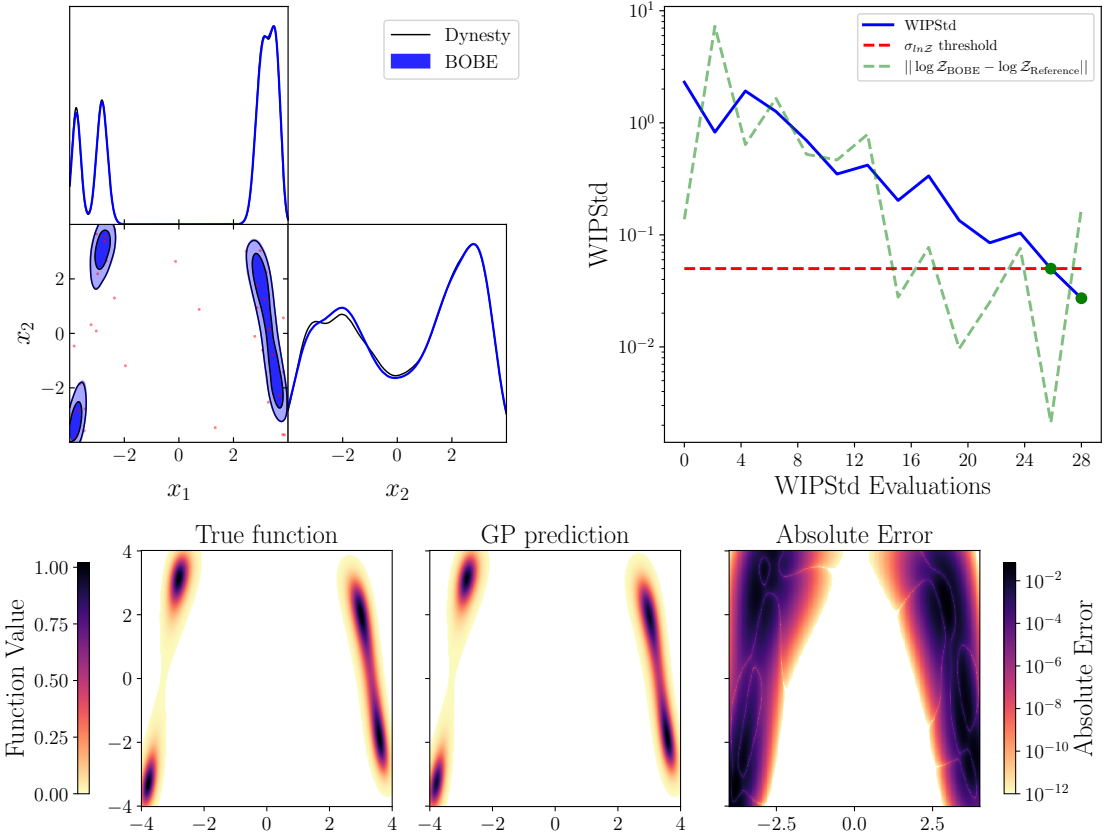


Figure 5. Same as Figure 3 for the Himmelblau function. This run was initialised with 8 Sobol samples.

the behaviour of the GP hyperparameters during the training process. We illustrate this for the example of a 6D Gaussian in Fig 8. The evolution of the correlation scales reveals two distinct regimes. An initial phase, characterised by strong fluctuations and marked differences between length scales for the different parameters, during which the rough shape of the posterior is being explored. This is followed by a second phase, where the different length scales have converged to a common value (as demanded by the symmetry of the problem), indicating a transition to an exploitation regime, i.e., the refinement of the emulator mostly in high-posterior regions of parameter space.

5.3 A cosmological application

Finally, we apply BOBE on an actual cosmological example, namely the base 6-parameter Λ CDM model, as well as its extension with non-zero spatial curvature, Λ CDM+ Ω_k . We consider the following likelihoods through their interface with Cobaya [78]:

- **CMB-lite**: a combination of the *Planck* 2018 low- ℓ temperature and polarisation likelihood [79], the *Planck-lite* nuisance-marginalised high- ℓ TTTEEE temperature and polarisation likelihood [79] and the *Planck* 2018 lensing likelihood [80].
- **CMB**: as above, but replacing *Planck-lite* with *Planck* high- ℓ **CamSpec** TTTEEE temperature and polarisation likelihood using **NPIPE** (*Planck* PR4) data [81], which adds 9 nuisance parameters.

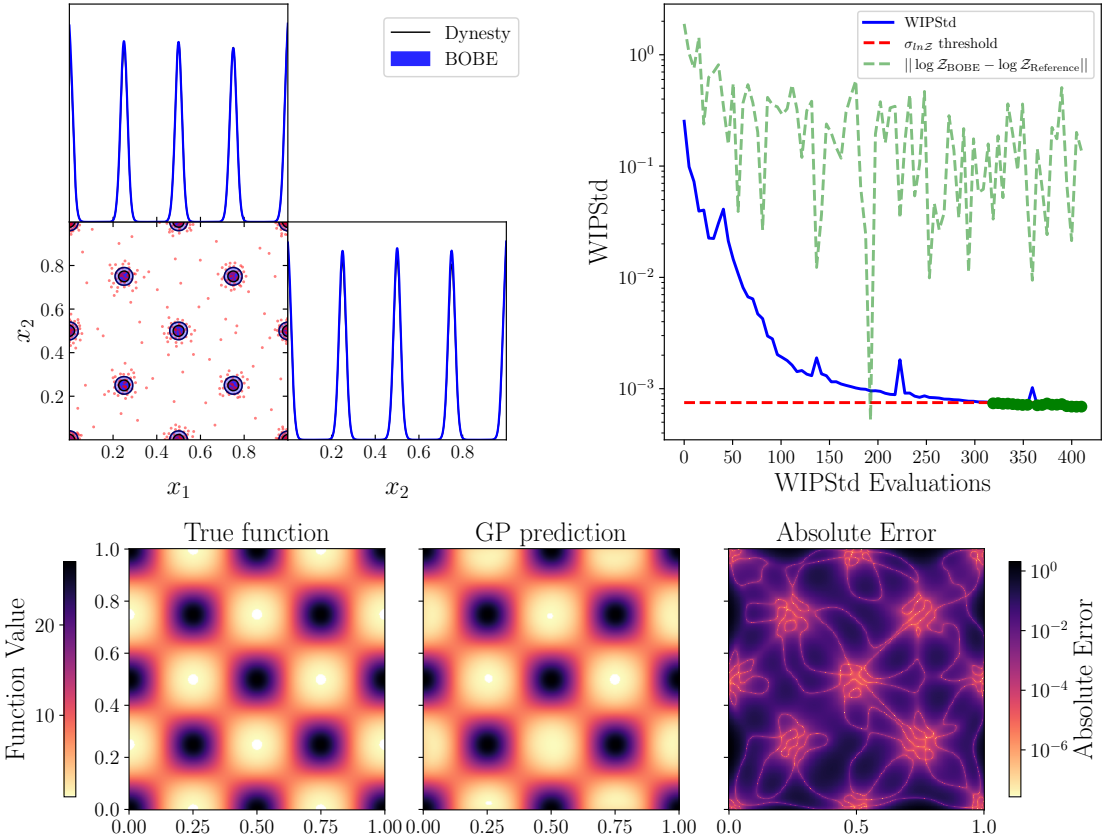


Figure 6. Same as Figure 3 for the Eggbox function. This run was initialised with 64 Sobol samples.

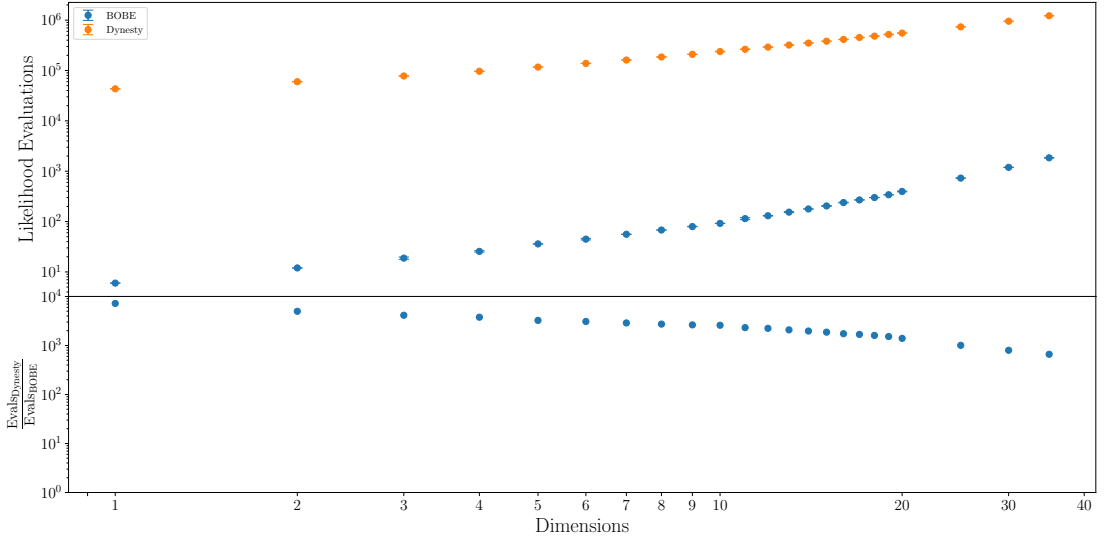


Figure 7. **Top:** Number of calls to an N -dimensional Gaussian likelihood/posterior required for BOBE to be trained (blue), compared with Dynesty, for an emulation/integration precision $\sigma_{\ln z} = 0.1$. **Bottom:** Ratio of the two numbers.

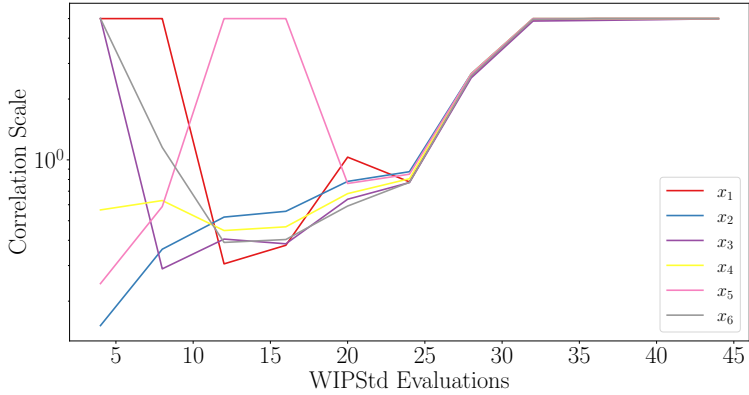


Figure 8. Evolution of correlation scale hyperparameters as a function of iteration from a **BOBE** run on a 6D Gaussian.

- **BAO:** Baryon Acoustic Oscillation (BAO) data from data release 2 of the DESI collaboration [82].

The prior ranges imposed on cosmological and nuisance parameters are listed in Table 5 in Section B. Cosmological observables required as input by these likelihoods are computed using the Boltzmann code **CAMB** [23].

We use a 2023 Apple M2 Pro with 10 cores and 32 GB of RAM for our computation. Thanks to parallelisation, the 10 cores can be efficiently used in their entirety, and **BOBE**'s memory requirements typically do not exceed 2-3 GB, even at a GP training set size of 1000+. All **BOBE** runs use batch acquisition and are initialised with a training set containing a combination of Sobol samples and samples drawn from a **Cobaya** reference distribution, with the details given in Table 3.

The convergence history and inferred 1- and 2-dimensional marginalised posteriors for the cosmological parameters are shown in Figure 9 for Λ CDM + CMB-lite, in Figure 10 for Λ CDM + CMB+BAO and in Figure 11 for Λ CDM+ Ω_k + CMB+BAO (see also Figures 12 and 13 in Section B for full posteriors including nuisance parameters). In all cases, the posteriors obtained from the **BOBE** emulator match those obtained from a nested sampling run on the actual likelihoods, demonstrating **BOBE**'s suitability for inference problems.

Model	Data	Sobol samples	Cobaya samples	Batch size
Λ CDM	CMB-lite	8	4	4
Λ CDM	CMB+BAO	32	8	5
Λ CDM+ Ω_k	CMB+BAO	32	16	5

Table 3. **BOBE** settings for cosmology runs.

For comparison, we also compute evidences with **PolyChord** (which is much faster than other nested samplers on the full CMB likelihood, due to its ability to exploit the difference between fast and slow parameters), using the actual likelihoods.

We list the **PolyChord** evidence estimates along with the results of our **BOBE** evidence computation in Table 4 – there is excellent agreement between the two for all combinations of model/data, but **BOBE** only took a fraction of the time to run on the same hardware. As

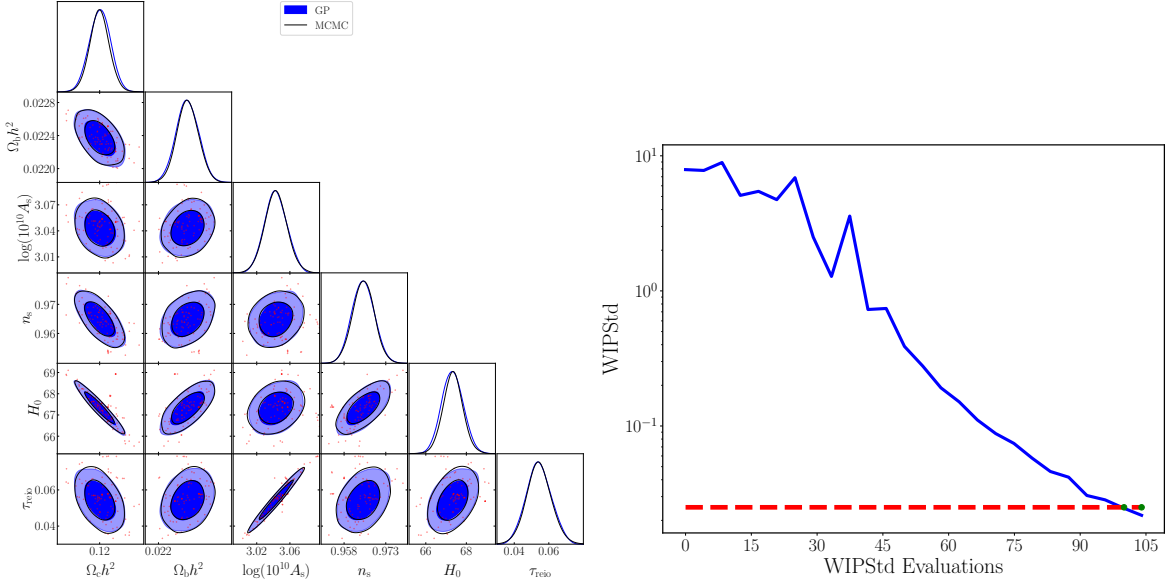


Figure 9. *Left:* Cosmological parameter posteriors for the Λ CDM model using the CMB-lite likelihood from the trained GP emulator (blue blobs/lines) compared to results from running MCMC on the actual likelihood (black lines). We also show the locations of training samples as red dots. *Right:* Evolution of WIPStd convergence diagnostic (blue line). The red dashed line denotes the convergence criterion.

already suggested by Figure 7, BOBE’s advantage is particularly pronounced in the lower-dimensional Λ CDM + CMB-lite case (3 min vs. 10 hours), but still substantial in the higher-dimensional problems involving the full CMB likelihood (54 min vs. ~ 1 day, and 2.5 hours vs. more than a day).

Model	Data	Samples	Wall time	$\ln \mathcal{Z}$ (BOBE)	$\ln \mathcal{Z}$ (PolyChord)
Λ CDM	CMB-lite	116	3 min	$-519.84 \pm 0.15 \pm 0.02$	-520.18 ± 0.32
Λ CDM	CMB+BAO	1213	54 min	$-5529.84 \pm 0.2 \pm 0.2$	-5529.65 ± 0.45
Λ CDM+ Ω_k	CMB+BAO	1713	2.5 hours	$-5529.93 \pm 0.24 \pm 0.22$	-5529.80 ± 0.37

Table 4. Results of BOBE cosmology runs. We quote both integrator and emulator uncertainties for the BOBE evidence estimate.

6 Conclusion

In this work, we have presented a Bayesian Optimisation framework for efficient Bayesian evidence estimation in cosmology and beyond, addressing the computational challenge of expensive likelihood evaluations. By combining Gaussian Process surrogates with our Weighted Integrated log-Posterior Standard Deviation (WIPStd) acquisition function, our method achieves accurate evidence estimates with up to three orders of magnitude fewer likelihood evaluations compared to traditional approaches. Further, the byproduct of efficient parameter inference makes this algorithm an even more attractive option for expensive likelihoods.

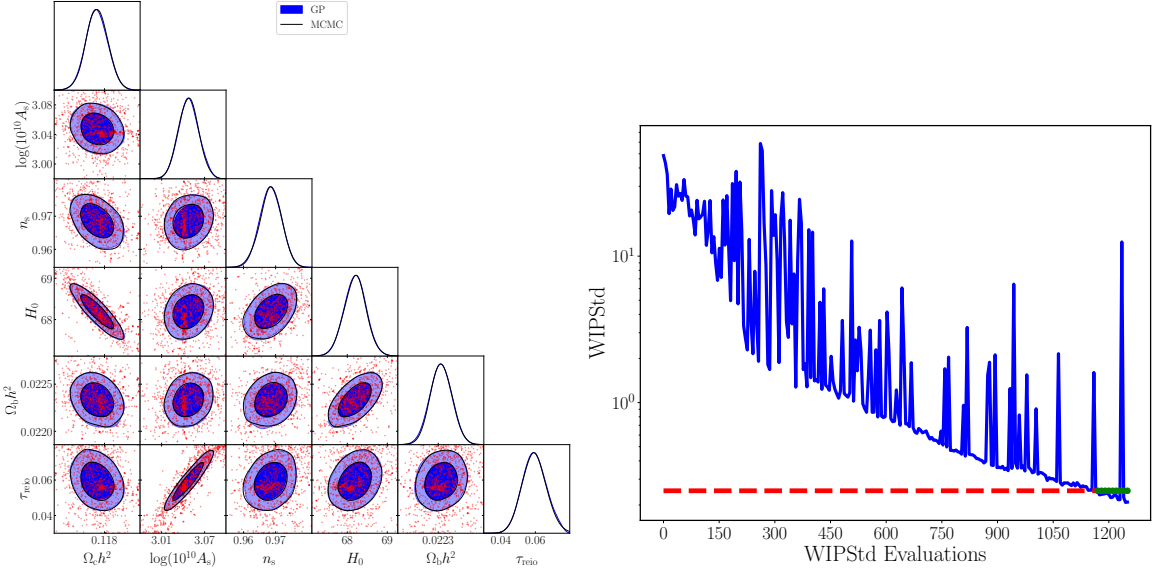


Figure 10. Same as Figure 9 for the Λ CDM model using the CMB+BAO likelihoods.

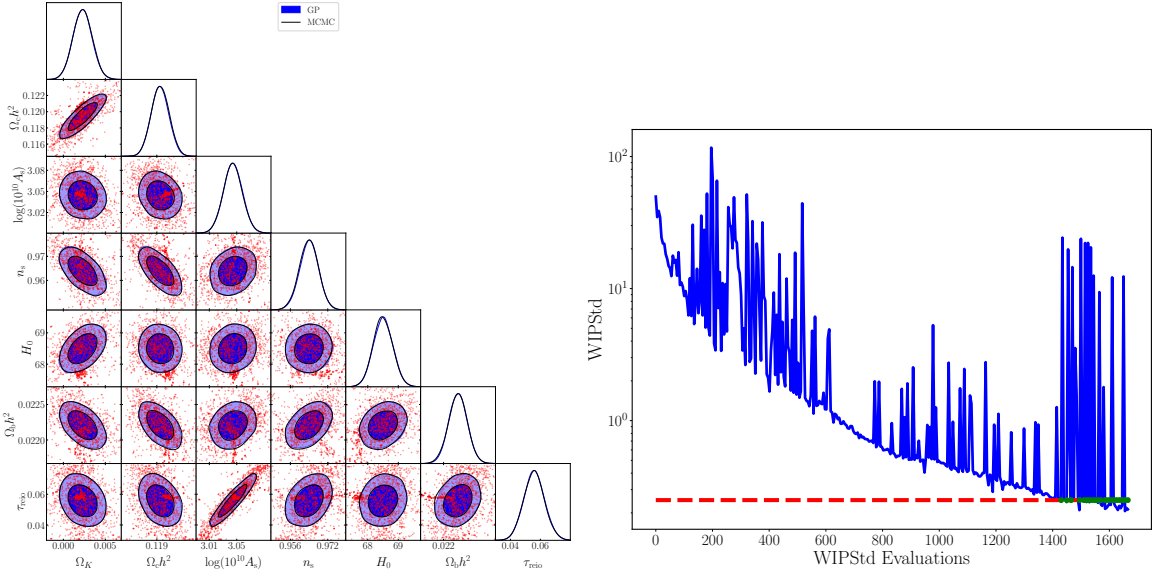


Figure 11. Same as Figure 9 for the Λ CDM+ Ω_k model using the CMB+BAO likelihoods.

By making use of an evidence aware strategy that ensures likelihood evaluations are guided by their impact on the precision of the evidence estimate, we have significantly reduced the number of true likelihood evaluations required to approximate the evidence to a given precision. The uncertainty quantification capabilities of GPs provide a natural convergence criteria based on the reduction of posterior-weighted standard deviation while the added combination of dynamic range compression through the choice of log-likelihood emulation and classifier guided exploration yields a robust and scalable framework. Future work could extend this framework by using richer Gaussian process constructions such as additive [83], sparse [84] random Fourier feature [85], deep kernels [86] or integrate multi-fidelity modelling

[87] to accommodate even higher dimensional parameter spaces.

We have applied our algorithm to various problems across different dimensionalities, from simple Gaussian likelihoods to multimodal, non-Gaussian test examples and most importantly realistic cosmological inference problems including Λ CDM and its extension with spatial curvature. Our framework can efficiently handle low to moderate-dimensional ($\lesssim 20$ D) parameter spaces, achieving significant efficiency gains over traditional Bayesian methods based on MCMC or nested sampling. This makes Bayesian model selection practical for computationally expensive scenarios where traditional sampling methods become prohibitive or even intractable. Overall, the combination of principled uncertainty quantification, active learning, and evidence-aware acquisition using BO provides a powerful tool for rigorous model comparison.

Acknowledgements

AM is partially funded by the STFC grant ST/X000648/1. AM also acknowledges the support of the Supercomputing Wales project, which is part-funded by the European Regional Development Fund (ERDF) via Welsh Government. NC acknowledges support from an Australian Government Research Training Program Scholarship. This research includes computations using the computational cluster Katana supported by Research Technology Services at UNSW Sydney. For the purpose of open access, the authors have applied a Creative Commons Attribution (CC BY) licence to any Author Accepted Manuscript version arising. Research Data Access Statement: our code, along with the scripts used to run the examples presented in this manuscript can be obtained from <https://github.com/Ameeek94/BOBE>.

A Classifier implementation

The classifier ensures that the emulator remains both accurate and tractable in high-dimensional settings. To set the log-likelihood threshold where we draw the classifier boundary, we follow the strategy used in `Gpry` [54]. This threshold strategy considers a posterior that is locally Gaussian in the region around the posterior maximum \mathbf{x}_0 in a d -dimensional parameter space. Under this assumption the posterior in the region \mathbf{x}_0 can be written as

$$p(\mathbf{x}) \propto \exp \left[-\frac{1}{2}(\mathbf{x} - \mathbf{x}_0)^\top \mathbf{C}^{-1}(\mathbf{x} - \mathbf{x}_0) \right], \quad (\text{A.1})$$

where C is the covariance matrix. The quadratic form can then be defined as

$$\Delta(\mathbf{x}) \equiv (\mathbf{x} - \mathbf{x}_0)^\top \mathbf{C}^{-1}(\mathbf{x} - \mathbf{x}_0), \quad (\text{A.2})$$

which follows a χ^2 distribution with N_d degrees of freedom,

$$\Delta \sim \chi_{N_d}^2. \quad (\text{A.3})$$

In one dimension a deviation of n_σ corresponds to a change in probability mass

$$p = \text{erfc} \left(\frac{n_\sigma}{\sqrt{2}} \right). \quad (\text{A.4})$$

In higher dimensions, the corresponding confidence region must enclose the same probability mass, which is achieved by requiring

$$P(\Delta \leq \Delta_d) = 1 - p \quad \text{and} \quad \Delta_d = \chi_{d,\text{isf}}^2(p) \quad (\text{A.5})$$

where $\chi_{d,\text{isf}}^2$ is the χ^2 inverse survival function with d degrees of freedom. So, an effective n_σ confidence region in d dimensions is defined by

$$\Delta_d(n_\sigma) = \chi_{d,\text{isf}}^2 \left(\text{erfc} \left(\frac{n_\sigma}{\sqrt{2}} \right) \right). \quad (\text{A.6})$$

This models the fact that the scale of an equivalent confidence region grows with dimensionality and, in the case of our algorithm, enables an approximation of what threshold from the peak is relevant to estimation of the evidence.

In our implementation we consider three complementary approaches, all of which draw a boundary relative to the current GP posterior maximum to determine admissibility using Equation (A.6). The first uses a Support Vector Machine (SVM) through the `scikit-learn` library [88] as also done in `Gpry` [54]. In addition to the SVM classifier, we implement a neural network based classifier using `Flax` [89], as well as a classifier that draws an ellipsoidal boundary centred on the current GP posterior maximum point. When the posterior is expected to be Gaussian or uni-modal, the ellipsoidal classifier provides the most accurate representation of its shape. For more complex posteriors, the SVM or neural network based classifiers are preferable as their greater flexibility allows them to adapt to more intricate posterior structures. In practice, the SVM offers the best performance on our hardware and is therefore selected as the default choice.

B Parameter priors and posterior plots

Parameter	Prior
Ω_k	[-0.010, 0.010]
$\Omega_c h^2$	[0.11, 0.13]
$\Omega_b h^2$	[0.021, 0.023]
$\ln(10^{10} A_s)$	[2.98, 3.10]
n_s	[0.94, 0.99]
H_0 [km s ⁻¹ Mpc ⁻¹]	[62, 72]
τ_{reio}	[0.03, 0.08]
<hr/>	
A_{143}^{power}	[0, 50]
A_{217}^{power}	[0, 50]
$A_{143 \times 217}^{\text{power}}$	[0, 50]
$\gamma_{143}^{\text{power}}$	[0, 5]
$\gamma_{217}^{\text{power}}$	[0, 5]
$\gamma_{143 \times 217}^{\text{power}}$	[0, 5]
A_{planck}	[0.9875, 1.0125]
c_{TE}	[0.950, 1.050]
c_{EE}	[0.950, 1.050]

Table 5. Prior ranges for the cosmological parameters of the Λ CDM and Λ CDM+ Ω_k models, as well as for the nuisance parameters required by the `Planck CamSpec` likelihood (below the dashed line). Prior ranges are chosen to be wide enough to remain non-informative relative to the posterior, while being narrower than typical MCMC parameter inference priors in order to ensure that the nested sampling algorithm converges within a reasonable number of steps.

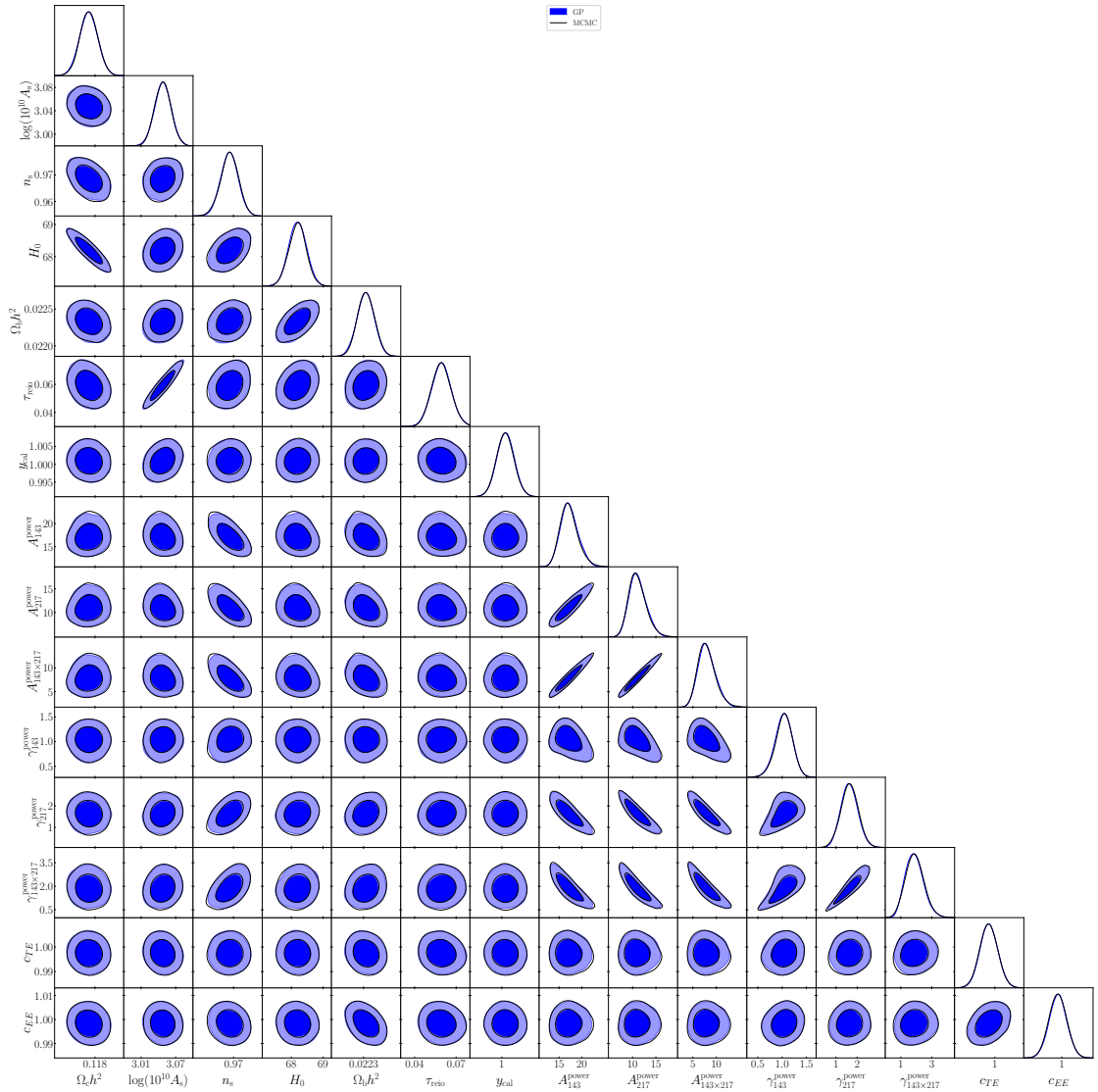


Figure 12. Cosmological and nuisance parameter posteriors for the Λ CDM model using the CMB+BAO likelihood from the trained GP emulator (blue blobs/lines) compared to results from running MCMC on the actual likelihood (black lines).

References

- [1] R. Trotta, *Applications of Bayesian model selection to cosmological parameters*, *Mon. Not. Roy. Astron. Soc.* **378** (2007) 72 [[astro-ph/0504022](#)].
- [2] R. Trotta, *Bayes in the sky: Bayesian inference and model selection in cosmology*, *Contemporary Physics* **49** (2008) 71 [[0803.4089](#)].
- [3] R. Trotta, *Bayesian Methods in Cosmology*, 1, 2017 [[1701.01467](#)].
- [4] H. Jeffreys, *Theory of Probability*, Oxford University Press (08, 1998), [10.1093/oso/9780198503682.001.0001](#).
- [5] J. Skilling, *Nested sampling for general bayesian computation*, *Bayesian Analysis* **1** (2006) 833.
- [6] F. Feroz, M.P. Hobson and M. Bridges, *MULTINEST: an efficient and robust bayesian*

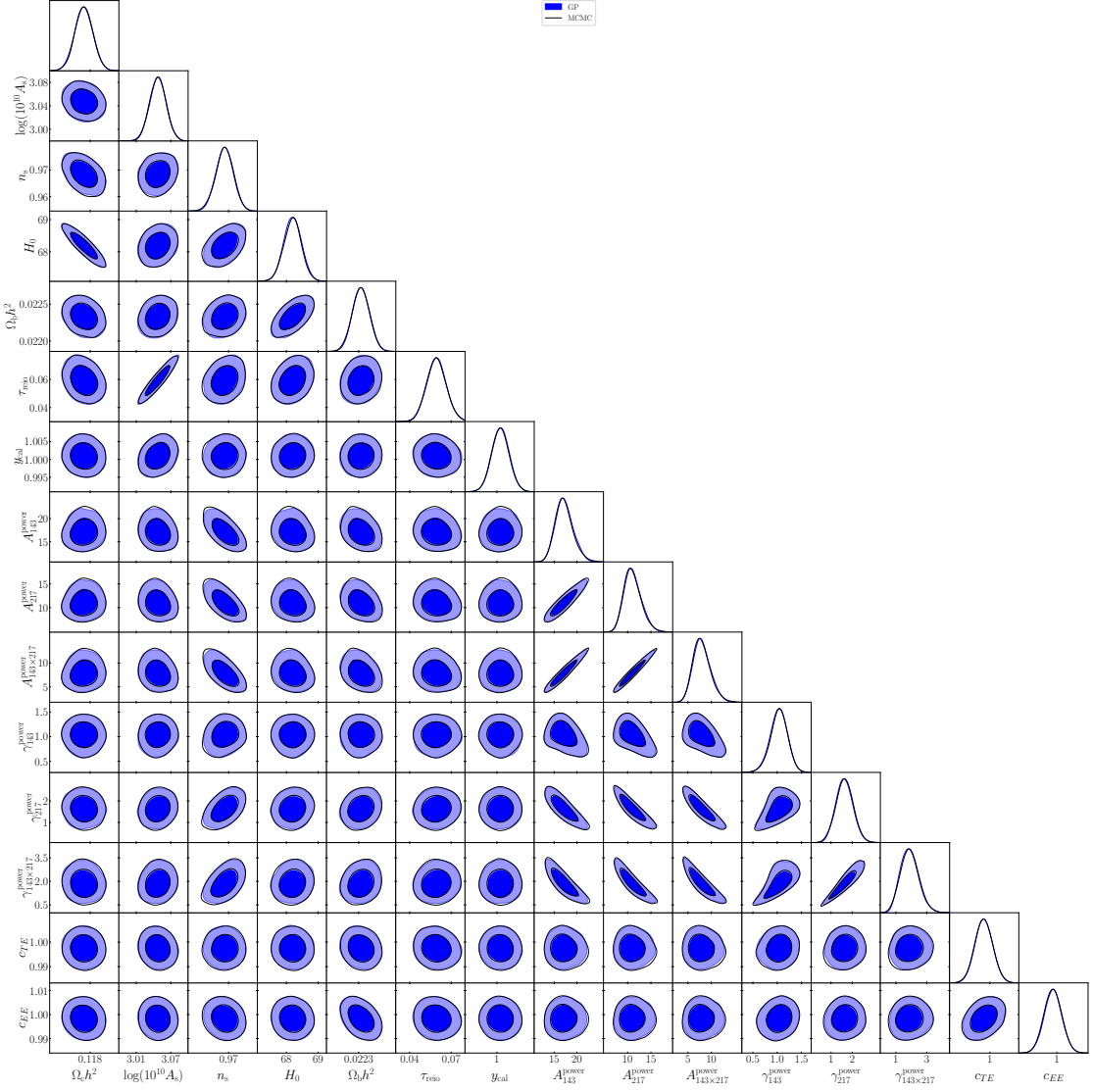


Figure 13. Same as Figure 12 for the Λ CDM+ Ω_k model.

inference tool for cosmology and particle physics, *Monthly Notices of the Royal Astronomical Society* **398** (2009) 1601 [[0809.3437](#)].

- [7] W. Handley, M.P. Hobson and A.N. Lasenby, *Polychord: nested sampling for cosmology*, *Monthly Notices of the Royal Astronomical Society: Letters* **450** (2015) L61 [[1502.01856](#)].
- [8] W. Handley, M.P. Hobson and A.N. Lasenby, *Polychord: next-generation nested sampling*, *Monthly Notices of the Royal Astronomical Society* **453** (2015) 4384 [[1506.00171](#)].
- [9] J.S. Speagle, *dynesty: a dynamic nested sampling package for estimating bayesian posteriors and evidences*, *Monthly Notices of the Royal Astronomical Society* **493** (2020) 3132 [[1904.02180](#)].
- [10] J.U. Lange, *nautilus: boosting Bayesian importance nested sampling with deep learning*, *Monthly Notices of the Royal Astronomical Society* **525** (2023) 3181 [<https://academic.oup.com/mnras/article-pdf/525/2/3181/51331635/stad2441.pdf>].

- [11] R.M. Neal, *Annealed importance sampling*, 1998.
- [12] A. Heavens, Y. Fantaye, A. Mootoovaloo, H. Eggers, Z. Hosenie, S. Kroon et al., *Marginal Likelihoods from Monte Carlo Markov Chains*, [1704.03472](https://arxiv.org/abs/1704.03472).
- [13] R.E. Kass and A.E. Raftery, *Bayes factors*, *Journal of the American Statistical Association* **90** (1995) 773 [<https://www.tandfonline.com/doi/pdf/10.1080/01621459.1995.10476572>].
- [14] J.D. McEwen, C.G.R. Wallis, M.A. Price and A.S. Mancini, *Machine learning assisted bayesian model comparison: learnt harmonic mean estimator*, 2023.
- [15] A. Polanska, M.A. Price, D. Piras, A. Spurio Mancini and J.D. McEwen, *Learned harmonic mean estimation of the Bayesian evidence with normalizing flows*, [2405.05969](https://arxiv.org/abs/2405.05969).
- [16] K. Lin, A. Polanska, D. Piras, A. Spurio Mancini and J.D. McEwen, *Savage-Dickey density ratio estimation with normalizing flows for Bayesian model comparison*, [2506.04339](https://arxiv.org/abs/2506.04339).
- [17] C.T.G. Sørensen, S. Hannestad, A. Nygaard and T. Tram, *Calculating Bayesian evidence for inflationary models using connect*, *JCAP* **03** (2025) 043 [[2406.03968](https://arxiv.org/abs/2406.03968)].
- [18] A. Lewis and S. Bridle, *Cosmological parameters from cmb and other data: A monte carlo approach*, *Physical Review D* **66** (2002) .
- [19] D. Foreman-Mackey, D.W. Hogg, D. Lang and J. Goodman, *<tt>emcee</tt>: The mcmc hammer*, *Publications of the Astronomical Society of the Pacific* **125** (2013) 306–312.
- [20] T. Brinckmann and J. Lesgourgues, *Montepython 3: boosted mcmc sampler and other features*, 2018.
- [21] G. Roberts and J. Rosenthal, *Optimal scaling for various metropolis-hastings algorithms*, *Statistical Science* **16** (2001) .
- [22] PLANCK collaboration, *Planck 2018 results. V. CMB power spectra and likelihoods*, *Astron. Astrophys.* **641** (2020) A5 [[1907.12875](https://arxiv.org/abs/1907.12875)].
- [23] A. Lewis, A. Challinor and A. Lasenby, *Efficient computation of CMB anisotropies in closed FRW models*, *Astrophys. J.* **538** (2000) 473 [[astro-ph/9911177](https://arxiv.org/abs/astro-ph/9911177)].
- [24] J. Chluba, J. Hamann and S.P. Patil, *Features and New Physical Scales in Primordial Observables: Theory and Observation*, *Int. J. Mod. Phys. D* **24** (2015) 1530023 [[1505.01834](https://arxiv.org/abs/1505.01834)].
- [25] V. Springel, R. Pakmor, O. Zier and M. Reinecke, *Simulating cosmic structure formation with the gadget-4 code*, *Mon. Not. Roy. Astron. Soc.* **506** (2021) 2871 [[2010.03567](https://arxiv.org/abs/2010.03567)].
- [26] M. Valentini and K. Dolag, *Hydrodynamic methods and sub-resolution models for cosmological simulations*, [2502.06954](https://arxiv.org/abs/2502.06954).
- [27] D.G. Figueroa, A. Florio, F. Torrenti and W. Valkenburg, *The art of simulating the early universe. part i. integration techniques and canonical cases*, *Journal of Cosmology and Astroparticle Physics* **2021** (2021) 035.
- [28] J.C. Aurrekoetxea, K. Clough and E.A. Lim, *Cosmology using numerical relativity*, *Living Rev. Rel.* **28** (2025) 5 [[2409.01939](https://arxiv.org/abs/2409.01939)].
- [29] R. Jimenez, L. Verde, H. Peiris and A. Kosowsky, *Fast cosmological parameter estimation from microwave background temperature and polarization power spectra*, *Phys. Rev. D* **70** (2004) 023005 [[astro-ph/0404237](https://arxiv.org/abs/astro-ph/0404237)].
- [30] W.A. Fendt and B.D. Wandelt, *Pico: Parameters for the Impatient Cosmologist*, *Astrophys. J.* **654** (2006) 2 [[astro-ph/0606709](https://arxiv.org/abs/astro-ph/0606709)].
- [31] E. Lawrence, K. Heitmann, M. White, D. Higdon, C. Wagner, S. Habib et al., *The coyote universe. iii. simulation suite and precision emulator for the nonlinear matter power spectrum*, *The Astrophysical Journal* **713** (2010) 1322–1331.

[32] H. Winther, S. Casas, M. Baldi, K. Koyama, B. Li, L. Lombriser et al., *Emulators for the nonlinear matter power spectrum beyond Λ CDM*, *Phys. Rev. D* **100** (2019) 123540 [[1903.08798](#)].

[33] J. Albers, C. Fidler, J. Lesgourgues, N. Schöneberg and J. Torrado, *CosmicNet. Part I. Physics-driven implementation of neural networks within Einstein-Boltzmann Solvers*, *JCAP* **09** (2019) 028 [[1907.05764](#)].

[34] EUCLID collaboration, *Euclid preparation: IX. EuclidEmulator2 – power spectrum emulation with massive neutrinos and self-consistent dark energy perturbations*, *Mon. Not. Roy. Astron. Soc.* **505** (2021) 2840 [[2010.11288](#)].

[35] K.R. Moran, K. Heitmann, E. Lawrence, S. Habib, D. Bingham, A. Upadhye et al., *The mira-titan universe – iv. high-precision power spectrum emulation*, *Monthly Notices of the Royal Astronomical Society* **520** (2022) 3443–3458.

[36] S. Günther, J. Lesgourgues, G. Samaras, N. Schöneberg, F. Stadtmann, C. Fidler et al., *CosmicNet II: emulating extended cosmologies with efficient and accurate neural networks*, *JCAP* **11** (2022) 035 [[2207.05707](#)].

[37] D. Piras and A. Spurio Mancini, *CosmoPower-JAX: high-dimensional Bayesian inference with differentiable cosmological emulators*, [2305.06347](#).

[38] S. Günther, *Uncertainty-aware and Data-efficient Cosmological Emulation using Gaussian Processes and PCA*, [2307.01138](#).

[39] S. Günther, L. Balkenhol, C. Fidler, A.R. Khalife, J. Lesgourgues, M.R. Mosbech et al., *OLE – Online Learning Emulation in Cosmology*, [2503.13183](#).

[40] W.-L. Loh, *On latin hypercube sampling*, *Annals of Statistics* **24** (1996) 2058.

[41] T.J. Santner, B.J. Williams and W.I. Notz, *The Design and Analysis of Computer Experiments*, Springer (2018).

[42] K.K. Rogers, H.V. Peiris, A. Pontzen, S. Bird, L. Verde and A. Font-Ribera, *Bayesian emulator optimisation for cosmology: application to the lyman-alpha forest*, *Journal of Cosmology and Astroparticle Physics* **2019** (2019) 031 [[1812.04631](#)].

[43] A. Nygaard, E.B. Holm, S. Hannestad and T. Tram, *Cutting corners: hypersphere sampling as a new standard for cosmological emulators*, *JCAP* **10** (2024) 073 [[2405.01396](#)].

[44] G. Aslanyan, R. Easther and L.C. Price, *Learn-As-You-Go Acceleration of Cosmological Parameter Estimates*, *JCAP* **09** (2015) 005 [[1506.01079](#)].

[45] C.E. Rasmussen and C.K.I. Williams, *Gaussian Processes for Machine Learning*, MIT Press, Cambridge, MA (2006).

[46] B. Shahriari, K. Swersky, Z. Wang, R.P. Adams and N. de Freitas, *Taking the human out of the loop: A review of bayesian optimization*, *Proceedings of the IEEE* **104** (2016) 148.

[47] P.I. Frazier, *A tutorial on bayesian optimization*, *arXiv preprint arXiv:1807.02811* (2018) [[1807.02811](#)].

[48] R. Garnett, *Bayesian Optimization*, Cambridge University Press (2023).

[49] L. Janken, S. Hannestad, T. Tram and A. Nygaard, *CLiENT: A new tool for emulating cosmological likelihoods using deep neural networks*, [2512.17509](#).

[50] J. Hamann and J. Wons, *Optimising inflationary features the Bayesian way*, *JCAP* **03** (2022) 036 [[2112.08571](#)].

[51] F. Leclercq, *Bayesian optimization for likelihood-free cosmological inference*, *Physical Review D* **98** (2018) 063511 [[1805.07152](#)].

[52] M. Pellejero-Ibañez, R.E. Angulo, G. Aricó, M. Zennaro, S. Contreras and J. Stücker, *Cosmological parameter estimation via iterative emulation of likelihoods*, *Mon. Not. Roy. Astron. Soc.* **499** (2020) 5257 [[1912.08806](#)].

[53] T. Takhtaganov, Z. Lukić, J. Müller and D. Morozov, *Cosmic Inference: Constraining Parameters with Observations and a Highly Limited Number of Simulations*, *Astrophys. J.* **906** (2021) 74 [[1905.07410](#)].

[54] J.E. Gammal, N. Schöneberg, J. Torrado and C. Fidler, *Fast and robust Bayesian inference using Gaussian processes with GPry*, *JCAP* **10** (2023) 021 [[2211.02045](#)].

[55] J. Torrado, N. Schöneberg and J.E. Gammal, *Parallelized Acquisition for Active Learning using Monte Carlo Sampling*, [2305.19267](#).

[56] A. Rocher, V. Ruhlmann-Kleider, E. Burtin and A. de Mattia, *Halo occupation distribution of Emission Line Galaxies: fitting method with Gaussian processes*, *JCAP* **05** (2023) 033 [[2302.07056](#)].

[57] D. Duvenaud, *Automatic model construction with Gaussian processes*, Ph.D. thesis, University of Cambridge, 2014. 10.17863/CAM.14087.

[58] V. Lalchand and C.E. Rasmussen, *Approximate inference for fully bayesian gaussian process regression*, in *Proceedings of The 2nd Symposium on Advances in Approximate Bayesian Inference*, C. Zhang, F. Ruiz, T. Bui, A.B. Dieng and D. Liang, eds., vol. 118 of *Proceedings of Machine Learning Research*, pp. 1–12, PMLR, 2020, <https://proceedings.mlr.press/v118/lalchand20a.html>.

[59] V. Lalchand, W.P. Bruinsma, D.R. Burt and C.E. Rasmussen, *Sparse gaussian process hyperparameters: Optimize or integrate?*, in *Advances in Neural Information Processing Systems*, 2022, <https://arxiv.org/abs/2211.02476>.

[60] M. Osborne, R. Garnett, Z. Ghahramani, D.K. Duvenaud, S.J. Roberts and C. Rasmussen, *Active learning of model evidence using bayesian quadrature*, *Advances in neural information processing systems* **25** (2012) .

[61] A.A. Gorodetsky and Y.M. Marzouk, *Merger kernels and integrated variance experimental design: Connections between gaussian process regression and polynomial approximation*, *SIAM/ASA Journal on Uncertainty Quantification* **4** (2016) 796 [[1503.00021](#)].

[62] R. Issa, S. Hamad, R. Grau-Crespo, E. Awad and T. Sparks, *Improving model generalizability in materials informatics via active learning with integrated posterior variance sampling*, *ChemRxiv* (2025) .

[63] J. Sacks, W.J. Welch, T.J. Mitchell and H.P. Wynn, *Design and analysis of computer experiments*, *Statistical Science* **4** (1989) 409.

[64] S. Crary and J. Stermann, *Four-point, 2d, free-ranging, imspe-optimal, twin-point designs*, *arXiv preprint arXiv:1510.01685* (2015) .

[65] S. Crary, *The nu class of low-degree-truncated, rational, generalized functions. i. imspe in design of computer experiments*, *arXiv preprint arXiv:1604.05278* (2016) .

[66] I. Sobol', *On the distribution of points in a cube and the approximate evaluation of integrals*, *USSR Computational Mathematics and Mathematical Physics* **7** (1967) 86.

[67] D. Eriksson and M. Jankowiak, *High-dimensional bayesian optimization with sparse axis-aligned subspaces*, 2021.

[68] P. Virtanen, R. Gommers, T.E. Oliphant, M. Haberland, T. Reddy, D. Cournapeau et al., *SciPy 1.0: fundamental algorithms for scientific computing in Python*, *Nature Medicine* **17** (2020) 261 [[1907.10121](#)].

[69] D. Phan, N. Pradhan and M. Jankowiak, *Composable effects for flexible and accelerated probabilistic programming in numpyro*, *arXiv preprint arXiv:1912.11554* (2019) .

[70] M.D. Hoffman and A. Gelman, *The no-u-turn sampler: Adaptively setting path lengths in hamiltonian monte carlo*, 2011.

[71] R. Barnes and A. Watson, *Efficient updating of kriging estimates and variances*, *Mathematical Geology* **24** (1992) 129.

[72] D. Ginsbourger, R. Le Riche and L. Carraro, *Kriging is well-suited to parallelize optimization*, in *Computational Intelligence in Expensive Optimization Problems*, Y. Tenne and C.-K. Goh, eds., (Berlin, Heidelberg), pp. 131–162, Springer Berlin Heidelberg (2010), DOI.

[73] C. Chevalier and D. Ginsbourger, *Corrected kriging update formulae for batch-sequential data assimilation*, 2012.

[74] C. Chevalier and D. Ginsbourger, *Fast computation of the multi-points expected improvement with applications in batch selection*, in *Learning and Intelligent Optimization*, G. Nicosia and P. Pardalos, eds., (Berlin, Heidelberg), pp. 59–69, Springer Berlin Heidelberg, 2013.

[75] T. Desautels, A. Krause and J.W. Burdick, *Parallelizing exploration-exploitation tradeoffs in gaussian process bandit optimization*, *Journal of Machine Learning Research* **15** (2014) 4053.

[76] D. Ginsbourger, R. Le Riche and L. Carraro, *A Multi-points Criterion for Deterministic Parallel Global Optimization based on Gaussian Processes*, .

[77] M.Z. Naser, M. Khaled al-Bashiti, A. Teymori Gharah Tapeh, A. Dadras Eslamlou, A. Naser, V. Kodur et al., *A Review of 315 Benchmark and Test Functions for Machine Learning Optimization Algorithms and Metaheuristics with Mathematical and Visual Descriptions*, *arXiv e-prints* (2024) arXiv:2406.09581 [2406.09581].

[78] J. Torrado and A. Lewis, *Cobaya: Code for Bayesian Analysis of hierarchical physical models*, *JCAP* **05** (2021) 057 [2005.05290].

[79] PLANCK collaboration, *Planck 2018 results. V. CMB power spectra and likelihoods*, *Astron. Astrophys.* **641** (2020) A5 [1907.12875].

[80] PLANCK collaboration, *Planck 2018 results. VIII. Gravitational lensing*, *Astron. Astrophys.* **641** (2020) A8 [1807.06210].

[81] E. Rosenberg, S. Gratton and G. Efstathiou, *CMB power spectra and cosmological parameters from Planck PR4 with CamSpec*, *Mon. Not. Roy. Astron. Soc.* **517** (2022) 4620 [2205.10869].

[82] DESI collaboration, *DESI DR2 results. II. Measurements of baryon acoustic oscillations and cosmological constraints*, *Phys. Rev. D* **112** (2025) 083515 [2503.14738].

[83] P. Rolland, J. Scarlett, I. Bogunovic and V. Cevher, *High-Dimensional Bayesian Optimization via Additive Models with Overlapping Groups*, *arXiv e-prints* (2018) arXiv:1802.07028 [1802.07028].

[84] A. Yang, *Scalable Bayesian Optimization with Sparse Gaussian Process Models*, *arXiv e-prints* (2020) arXiv:2010.13301 [2010.13301].

[85] M. Mutný and A. Krause, *Efficient high dimensional bayesian optimization with additivity and quadrature fourier features*, in *Proceedings of the 32nd International Conference on Neural Information Processing Systems*, NIPS’18, (Red Hook, NY, USA), p. 9019–9030, Curran Associates Inc., 2018.

[86] M. Wistuba and J. Grabocka, *Few-Shot Bayesian Optimization with Deep Kernel Surrogates*, *arXiv e-prints* (2021) arXiv:2101.07667 [2101.07667].

[87] J. Song, Y. Chen and Y. Yue, *A General Framework for Multi-fidelity Bayesian Optimization with Gaussian Processes*, *arXiv e-prints* (2018) arXiv:1811.00755 [1811.00755].

- [88] F. Pedregosa, G. Varoquaux, A. Gramfort, V. Michel, B. Thirion, O. Grisel et al., *Scikit-learn: Machine learning in Python*, *Journal of Machine Learning Research* **12** (2011) 2825.
- [89] J. Heek, A. Levskaya, A. Oliver, M. Ritter, B. Rondepierre, A. Steiner et al., *Flax: A neural network library and ecosystem for JAX*, 2024.